10-30-2015

Passive Symmetry in Dynamic Systems and Walking

Haris Muratagic
University of South Florida, muratagic@mail.usf.edu

Passive Symmetry in Dynamic Systems and Walking

by

Haris Muratagić

A thesis submitted in partial fulfillment
of the requirements for the degree of
Master of Science in Mechanical Engineering
Department of Mechanical Engineering
College of Engineering
University of South Florida

Major Professor: Kyle B. Reed, Ph.D.
Rajiv Dubey, Ph.D.
Seok Hun Kim, Ph.D.

Date of Approval:
October 23, 2015

Keywords: Gait Symmetry, Uncoupled Synchronization, Gait Modeling,
Passive Dynamic Walkers, Nonlinear Systems

Acknowledgments

I would like to express my deep gratitude to Dr. Kyle B. Reed for allowing me to work in his laboratory and for being a great mentor and advisor. Through working in his lab I have gained invaluable skills and experience that I will take with me into my engineering career and beyond. I also want to thank everybody that works in the REED laboratory; they not only inspired me with their work ethic and positive attitudes, but were also there to help me develop various projects.

I would like to thank my siblings, Amira, Amir, and Maida for all the support and help that they have given me throughout my academic career. Thanks to my older brother for always asking me math questions and annoying me to the point where I became better at math than him. Thanks to my parents for always pushing me to set high academic goals and reach for the highest academic achievements, even if it was just to catch up to Maida.

Finally, I would like to thank Dr. Ismet Handzic for all that he has done to help me become a better engineer. Without his guidance I would not have become a researcher or graduate student, and my figures would have never looked presentable.

Table of Contents

List of Tables

List of Figures

Abstract

The ubiquitous nature of symmetry lends itself to be taken for granted, however the breath of research on symmetry encompasses several disciplines. In engineering, studies centered on symmetry often address issues in dynamic systems theory, robotics, and gait rehabilitation. This thesis presents findings on two specific topics dealing with passively induced symmetry; dissimilar rotating systems and human gait. Past studies on passive symmetry in dynamic systems often incorporate physical coupling or a controller. This thesis presents a technique to passively induce symmetry between two dissimilar systems that are not physically connected. This work also presents a human gait study consisting of several elements that merge to provide a unique look at how walking symmetry and altered physical parameters (leg length and added weight) of the lower limbs are related.

One aspect of this thesis shows the successful development of a general method to induce synchronization between any two dissimilar, uncoupled, rotating systems given the same degrees of freedom, initial angular dynamics, and applied torque. This method is validated with a simulation and subsequent comparison with two physical experiments. The results are in agreement, with slight variations due to the friction and damping of the physical systems. This is further expanded to include the induced symmetry of two systems that experience an external collision. Due to the highly non-linear nature of such systems, an analytical solution was not found; instead a numerical solution is presented that resulted in partial symmetry between systems.

The gait study demonstrated that weighted walking and altered leg length have both independent and combined spatio-temporal effects on lower limb symmetry. While altered leg length alone resulted in higher gait asymmetry, the combination of the two physical changes increases this asymmetry to affect the same limb. This study also showed that cognitive and physically distracted

walking does not have an added effect to the gait symmetry with passive physical changes. In addition, this study was able to demonstrate that the arm swinging that occurs during natural walking does not significantly alter spatial or temporal gait parameters.

Chapter 1: Introduction

In its clearest and simplest form, symmetry is defined as an agreement of pattern and proportion. Our affinity for symmetry is so deeply entrenched in our lives that it may impede our ability to discern how universal and important it is. For instance, studies have shown that attractiveness is highly influenced by how symmetric certain facial attributes are [52]. In engineering, symmetry is usually synonymous with stability and efficiency. Several disciplines of mechanical engineering such as dynamics, robotics, and rehabilitation encourage symmetric or synchronized systems. Symmetry is thought to enable efficient task performance, such as in gait. A symmetric walk allows us to stably move from place to place without feeling overburdened and uncomfortable. However, imbalances of gait do often exist in human gait, and one common example is a person who has suffered from a stroke. They lack the equilibrium of a normal gait because of a condition called hemiparesis, where one side of their body becomes paralyzed [33, 43]. There are several training methods to improve this condition, but our aim is to improve the symmetry of such impaired gaits with passive means. This research aims to explore the induced symmetry in dynamic systems and human walking and how this symmetry can be introduced back into unsynchronized or unbalanced dynamic systems and humans.

This thesis begins with a background chapter that will provide a review of the research surrounding the synchronization and symmetry of dynamic systems and passive walking models. The background will present historical examples on symmetry and then expand to demonstrate the variety of research that is performed in the realm of symmetry today. Throughout the background I will be highlighting just how powerful the topic of symmetry and synchronous systems are in engineering. Finally, I will survey some of the walking studies that have inspired this research and explain how this thesis can provide an additional insight to the field.

Chapter 3 then introduces a general synchronization method that was developed to accurately predict and match the motion between two dissimilar rotating systems. The synchronization of any two rotating systems can be as simple as physically placing a joining spring or damper between the systems or may require sophisticatedly controlled actuators that augment natural system dynamics. However, this research focuses on *dissimilar* rotating systems *without* any physical coupling. The passive kinematic matching technique allows two independent systems to generate the same motion without any physical system coupling or actuator control law. To validate this method, the passive synchronization technique is applied to two open-ended rotating kinematic chains: single- and double- link pendulums with different masses at different mass locations along the links. Even though double-link pendulums are highly nonlinear systems that are sensitive to changes in initial conditions and system parameters, this matching technique enables the same generated motion on dissimilar double-link pendulums.

The practical application of such a passive matching technique is the flexibility in mechanical design as one is able to describe the same kinematics with a variety of parameters (i.e., masses and mass distributions). In essence, one is able to decouple the mass and the first moment and second moment of inertia so systems with dissimilar masses and mass distributions will have the same motion. For example, the motion of a double-link pendulum modeled as two links with one mass per link can only be described by one unique combination of masses and mass locations along the links. However, having two masses per link allows the kinematics to be described with an infinite number of distinct systems with distinct masses and mass distribution that all have the same resulting motion. In fact, the minimum number of masses per rotating link to describe any arbitrary rotational kinematics is two masses, yet many models only include one mass. Using only one mass per link inherently couples the moments of inertia so that any change in the location of the mass necessarily affects both the first and second moments of inertia.

The modeling method to derive this synchronization technique can be used to simplify complicated rotational kinematics problems by simplifying the dynamics model of the system by assuming a finite distribution of point masses along swinging members. For example, the rotation

of a fan blade can be represented with two masses distributed as specified using this method instead of finding detailed masses, mass distributions, or moments of inertias of the continuous system. This type of modeling can also be applied to human or robotic limbs and in prosthesis design.

The research is then expanded further to form synchronization examples of dynamic systems that experience external collisions. The inclusion of the collision equations to these systems introduce complex dynamics, thus increasing difficulty in synchronization. The same double pendulum systems are used, but due to the complexity, a numerical solution is presented. When inverted, these types of systems can be viewed as simple Passive Dynamic Walkers (PDW), which are often used in gait rehabilitation research to model the physical motion of human walking.

PDWs allow engineers to study the natural gait in a purely physical sense without the interaction or response of the conscious motor control. However, this research aims to tie together the passive synchronization methods previously discussed and the symmetry or asymmetry present in human gait that inherently involves this conscious factor. One major issue with comparing applied passive changes in simulations and human walking is that these simulations cannot account for what the conscious effects will do to the gait pattern. To investigate this problem and to identify which type of passive changes (leg length or leg weight) are most effective to human subjects, a gait symmetry experiment was developed.

Chapter 4 presents a multi-component walking study on the induced symmetry of human walking. One major element of this study is the testing of different combinations of passive changes. These passive changes consist of adding a weight to the ankle of the weaker foot and changing the leg length of the plant, or strong leg. The first investigation of this study allowed us to see how such passive changes affect the symmetry of gait, and what combination of either leg length or weight change produces a more symmetric gait in physically asymmetric configurations. Certain asymmetric configurations that are able to exhibit a symmetric gait, have huge implications for improving symmetry and efficiency of people that have an altered gait.

Another element to this study is the testing of how these passive physical differences affect a human walk when the subjects perform a distracting physical and cognitive task. Ruffieux et

al. [44] conducted a large scale literature review of dual task performance studies and concluded that additional research is required to study what affects it has on performance in young adults. The dual task distracted walking in this thesis attempts to minimize the conscious effects of each participant, thus allowing the body to walk naturally, or to exhibit a truly passive gait. This research can be applied to study the effects that distractions have on gait symmetry. For instance, cell phone use while walking might result in an unsynchronized and inefficient gait. This study can also show how asymmetric arm swinging motion, such as when performing a carrying task, influences gait parameters.

Chapter 2: Background

Evidence shows that symmetry has been a prevalent aspect of life dating back to ancient times when it was used in artistic expression (shown in Figure 2.1) and communication [26]. Since then, symmetry has been an intriguing concept that has represented the order and beauty often present in nature. The idea of symmetry was first introduced by the Greeks to describe certain charecteristics of well proportioned art and artifacts that were present all around them [26]. Today, research on symmetry has expanded exponentially, and it is studied throughout many disciplines including art [1], materials engineering [51], physics [47], and even psychology [34].

Symmetry in engineering is often synonymous with balanced and efficient systems. Marsden et al. [36] stated that "Symmetry has always played an important role in mechanics, from

Figure 2.1: An engraving on the Raimondi Stele from the ancient Chavin culture. This artifact shows the vast symmetry present in early art-forms [Public Domain] [53].

fundamental formulations of basic principles to concrete applications". To better predict the behavior of their systems, mechanical engineers often design symmetric and balanced machines and components. Engineers also are interested in studying how such symmetry can be induced in dynamic systems, particularly dissimilar ones. There has been extensive research on how symmetry, or synchronization, can be established between two asymmetric systems, with the earliest beginning in the 17th century.

2.1 Physically Induced Synchronization

In 1657 Mathematician Christiaan Huygens invented the first pendulum clock in search of improvements to nautical navigation [4]. These pendulum clocks were an impressive and advanced mechanism during this time period. One distinct characteristic of these clocks is that when hung on the same wall they tend to synchronize over time. Huygens concluded this phenomenon was due to the small transfer of movement between clocks through the supporting structure. This clock phenomenon can be regarded as the first observation of a *coupled synchronized* oscillator.

As part of the rise of faster computing power came the ability to actively synchronize coupled mechanical systems with linear, nonlinear, passivity-based, or active control laws. There are hundreds of publications which demonstrate such control laws, some of these publications are on controlled motion synchronization for gyroscopes [40], inverted pendulum systems [38], and chaotic systems [30].

Passive kinematic synchronization has had very limited exposure despite numerous articles addressing coupled synchronization. This includes Huygens' clock phenomenon and recent studies such as the synchronization of coupled oscillators [8], analysis of coupled multi-pendulum systems [11], and matching of coupled double pendulums under the effects of external forces [29]. In fact, the only publications I discovered that dealt with passive synchronization were based in sports science.

2.2 Passive Uncoupled Synchronization

A golfer's technique and the use of familiar equipment are essential features of optimal performance. It is for this reason that all golf clubs in a set are matched (synchronized) statically and dynamically, so when swung, each club behaves and feels the same to the golfer [3]. Statically a golf club is matched by simply balancing it on a fulcrum, however dynamically matching the golf club can be achieved by matching the moment of inertia for each club in the set about the swinging axis [10]. Jorgensen presents a golf club dynamic synchronization technique by modeling the swing arm and golf club and matching overall moments of inertia about the wrist axis [27]. In these examples the kinematics of each uncoupled system (golf club) is synchronized given the same input torque (the golfer's swing). While this technique of golf club matching is practical in its specific application, it lacks generalization and flexibility to apply to other rotating systems to be synchronized.

Although limited literature addressing the field of passive synchronization of uncoupled systems exists, a generalized passive synchronization method for physically uncoupled rotating systems has practical implications. For example, the motion of human, insect or robotic arms can be matched to improve the performance of certain tasks, such as lifting an object. A general method could also impact several other fields including locomotion robotics, lower limb prosthetic devices, lower limb rehabilitation and gait analysis.

In gait rehabilitation, for instance, an individual's walk can largely be modeled as two inverted pendulums (left and right step) rotating about the stance foot and progressing down a decline with gravity as the only source of energy [32]. Being able to induce symmetry in such systems has huge implications for improving gait rehabilitation models, simulations, and analysis. Such models, illustrated in Figure 2.2, are called passive dynamic walkers (PDW) and have been shown to predict certain aspects of human gait dynamics [13, 21, 22] and are commonly used to simulate walking.

Figure 2.2: A three link physical passive dynamic walker example with rounded feet.

2.3 Symmetry in Walking

2.3.1 Passive Dynamic Walkers

PDWs have long been utilized in the simple modeling of the dynamics of human gait. They are a preferred method of gait modeling due to their repeatability and their ability to simulate physical gait dynamics [12]. They are also popular because they can exhibit the asymmetries that are present within a person's gait without requiring to physically measure their walk. For instance, if a person has interesting physical characteristics present in their lower limbs, a PDW can be used to model their gait and investigate any asymmetries in their walk. In addition, the model can be used to evaluate the usefulness or legitimacy of different rehabilitation methods that can be applied.

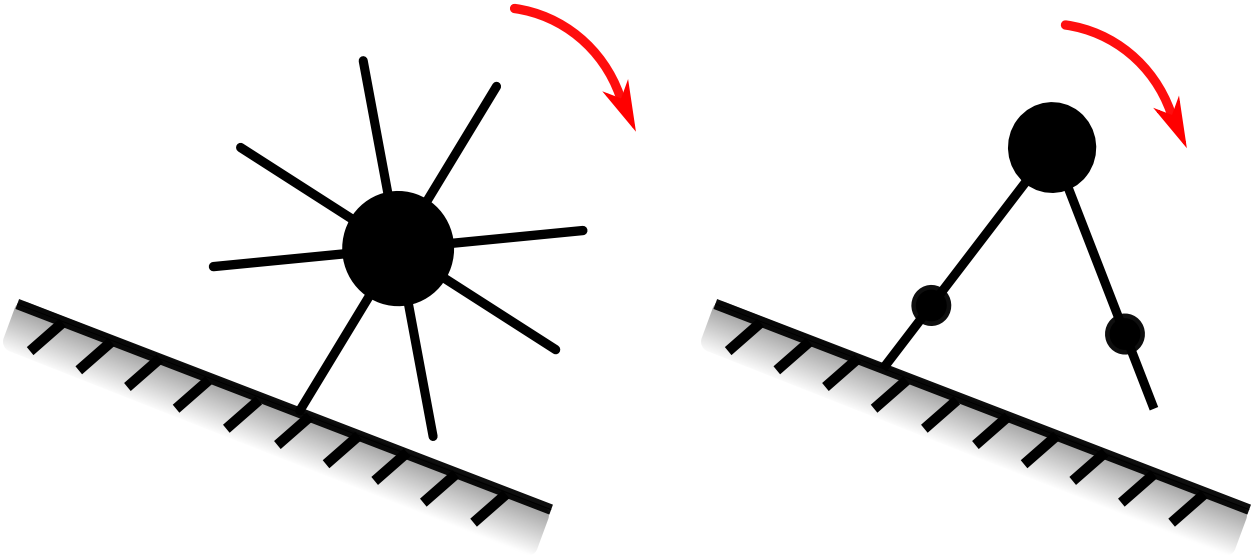

(a) (b)

Figure 2.3: McGeer's developments in passive dynamics. (a) The rimless wheel concept showing the transfer of energy that occurs in walking (b) The compass gait used to model simple human gait

Several of these models have been developed, and they include both physical representations and computer simulations.

The study and expansion of PDWs has steadily increased in recent years, but the most notable developments have come from Tad McGeer. McGeer developed the rimless wheel concept, shown in Figure 2.3a, that considered inelastic collisions of each spoke at the point of contact and provided insight into how to develop simple walking models. With this concept he developed a two link walker, called the compass gait model that was able to successfully represent the energy transfer that occurs during walking as the heel of the foot collides with the ground [37]. However, this model was too simple to be used to represent the complex human gait. Chen used this model to develop a five mass PDW, illustrated in Figure2.4, that included hip, thigh, and shank masses with a linkage system. The five mass model included knee collision equations which allowed for a more accurate representation of the human gait [5]. These advancements gave way to several other studies in passive walkers including some centered on symmetry.

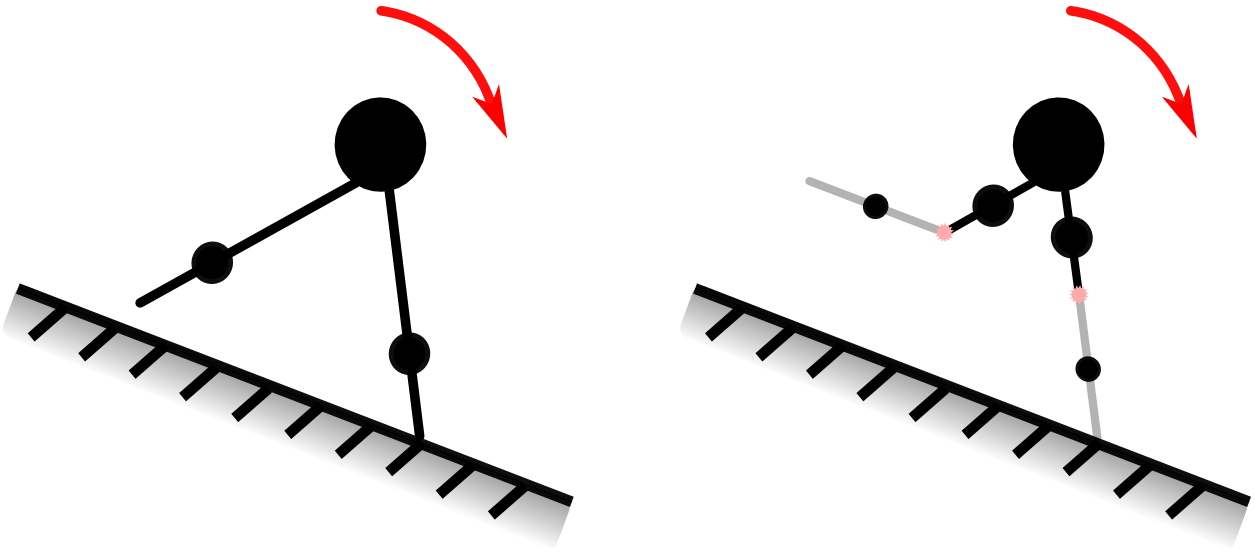

(a) (b)

Figure 2.4: The evolution of the compass gait. (a) The original compass model (b) improved design with knee and heel strike collisions.

Honeycutt et al. [25] used a brute force search through a numerical PDW model to show that asymmetric limbs can have symmetric kinematics. In addition, they were able prove that lowering a prosthetic knee joint while lowering the prosthetic mass can result in a spatially symmetric gait. Gregg [16, 17] examined symmetry from the other point of view by finding symmetric PDW parameters that yielded asymmetric kinematics. A leg synchronization technique can be helpful to design and implement devices and methods for PDWs, general walking robots (shown in Figure 2.5), and individuals. Such methods might include evening out gait asymmetries [14], or intentionally exaggerating gait asymmetries for rehabilitation [19, 42]. One area where such models would be useful would be in post stroke gait rehabilitation.

2.3.2 Asymmetry in Humans

Stroke is a condition most commonly caused by a suspension of the blood supply to the brain, depriving it of oxygen and other vital nutrients. When a person suffers a stroke they often develop physical asymmetries (shown in Figure 2.6), including asymmetric gait, arm swinging,

and facial features [48]. They experience diminished strength in the affected limbs causing the hemipartic gait to be inefficient and difficult to stabilize [39]. There are several rehabilitation methods that have been developed recently to induce symmetry back into a patient post-stroke, the most common being split belt treadmill training. This type of training increases a particular asymmetry, such as step length, on post stroke patients by applying different speeds to the tread belts. The body of the patient then adjusts to accommodate this exaggerated asymmetry, and ideally after several minutes, the body will adapt to this new change [49]. When the belt speeds are returned to normal, their gait will exhibit a more symmetric pattern depending on what parameters were affected. Although this method has been successful, one major issue is the need for this

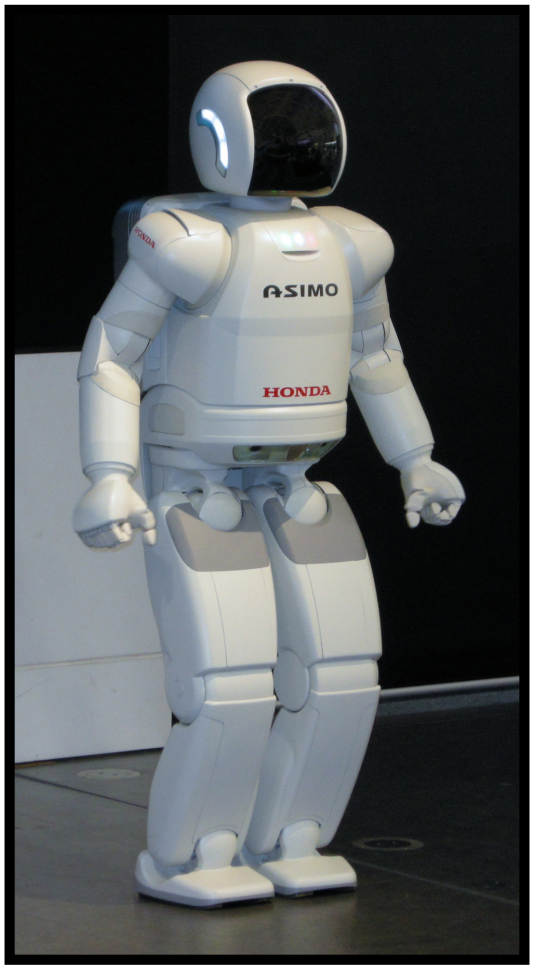

Figure 2.5: An example of a bipedal robot. These types of walking robots can benefit from further PDW research and advancements [Public Domain] [23].

equipment. A patient must visit the clinic for every training session, which inherently becomes time consuming and a financial burden.

This thesis aims to investigate how changing physical parameters at certain locations can alter the interaction of gait parameters, specifically the step length, step time, and three ground reaction forces. These physical changes, weighted walking and single leg length increase, are applied in several different combinations and all are analyzed. Previous research on weighted walking and unbalanced leg length have been partially addressed, but the simultaneous effect that they have on gait symmetry has not.

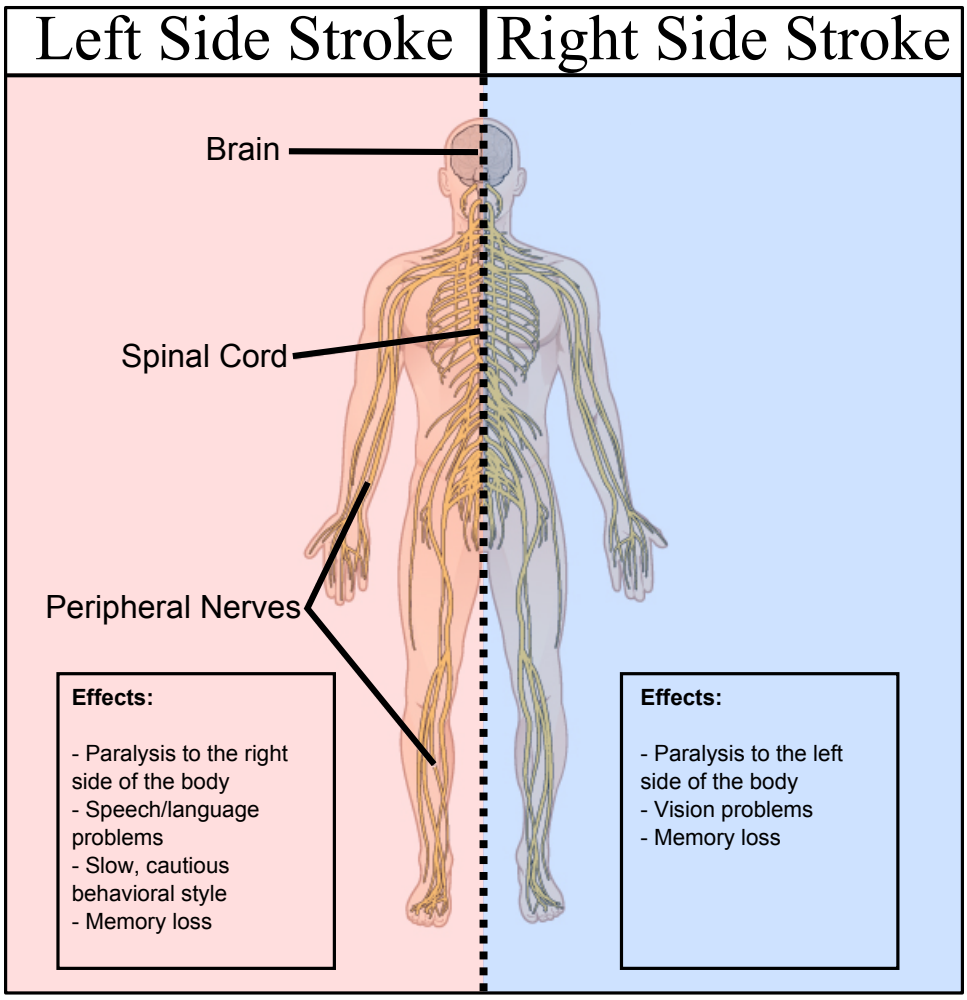

Figure 2.6: An overview of the effects of both left and right sided strokes.

Weighted walking is commonly studied in the fields of mobility rehabilitation [7], general strength training [15], and assessing aerobic ability [31]. While such topics have been extensively researched in the realm of rehabilitation, only two research articles were found that addressed how weighted walking alters gait. Skinner et al. [46] analyzed gait and oxygen consumption of people wearing symmetric and asymmetric weights. They were able to show that asymmetrically applied weights changed the stance phase of the weighted limb, while symmetrically applied weights cause little to no change. Another study looked at what affects weighted garments had on balance and gait in stroke patients [41]. The results show no significant change to either balance or gait symmetry with weighted walking. Although these studies give some insight on the changing of gait parameters in weighted walking, they lack the addition of leg length change and how the two interact to modify gait.

Asymmetry in lower limb lengths is commonly referred to as leg length discrepancy (LLD), and it affects up to 70 percent of the population [18]. Although the majority of people affected by it only possess a small LLD, there are portions of the population with large and burdensome LLD. Such large differences in limb length cause a multitude of physical problems, most commonly gait asymmetry. Due to it prevalence, the relationship between gait symmetry and LLD has been extensively studied. Several studies have found that as the LLD in able-bodied subjects increased so does the gait asymmetry [28, 45]. Despite such studies showing the correlation between LLD and gait symmetry, no research has been conducted on the induced gait symmetry that results from different combinations of applied LLD and single leg weighted walking.

Aside from studying how these physical changes work together in altering gait symmetry, this work also investigates the effect that dual task walking has on these changing physical parameters. Subconscious walking of human gait can be adequately modeled by the PDWs, mentioned earlier, but one major flaw of these models is the lack of the consideration for the consequences of human behavior that occurs during walking. The act of walking is driven by muscles that are controlled by the nervous system, so not considering these factors can result in inaccurate models. Attempting to simulate the reaction of the nervous system during walking would be a very

complex process, but limiting the conscious side effects during a walking study would not. These types of studies do exist, however they are primarily considering the after effects and adaptation of performing dual task or distracted walking in post stroke subjects.

Malone et al. [35] tested the differences in adaptation in conscious and distracted correction of walking. The study found that subjects that were distracted during the experiment exhibited longer aftereffects, however these only affected spatial parameters of gait. Although the study observes the conscious and dual task effect during correction of walking, it does not test how induced physical asymmetry alters the symmetry in gait between the two types. Other dual task gait studies have looked at the increase in falling risk [24], the effectiveness of dual task based exercise in stroke patients [50], and others [9].

As a consequence of the dual task walking study presented in this thesis, the influence of asymmetric arm swinging on gait is also investigated. On several occasions the arm swinging that naturally occurs during walking is obstructed, as compared in Figure 2.7. For instance, walking

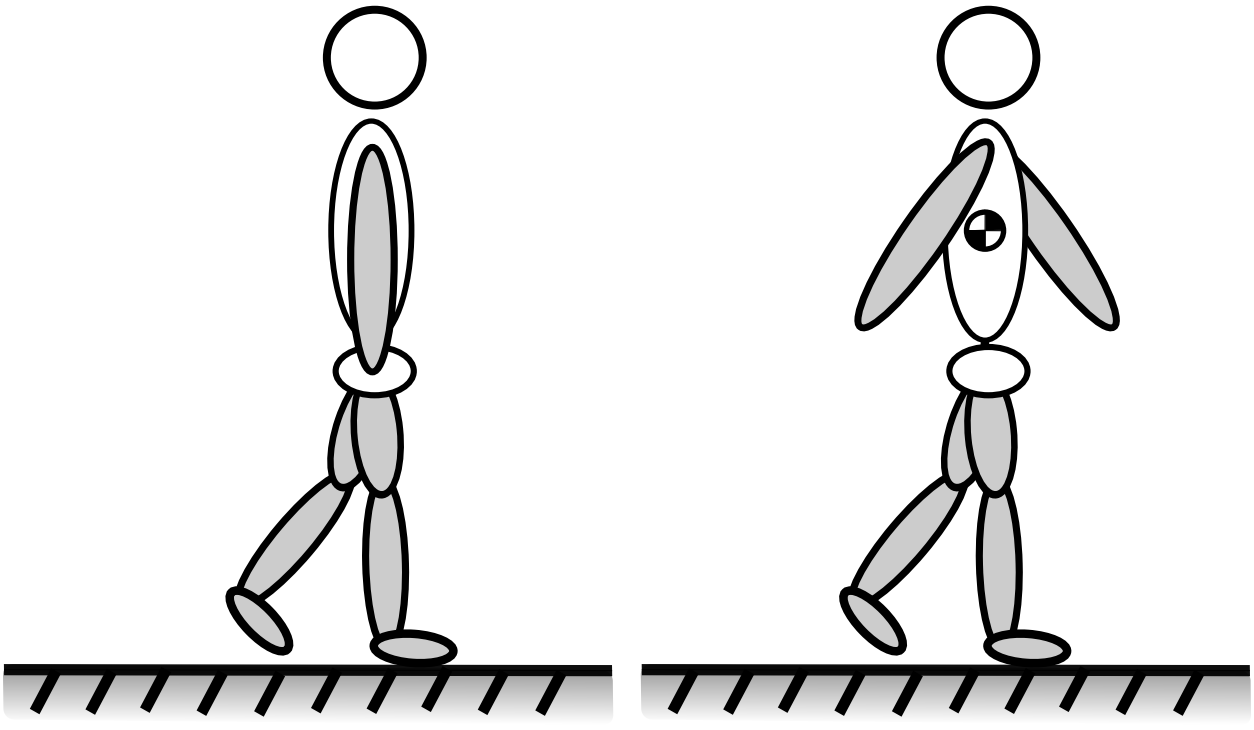

Figure 2.7: Differences in arm swinging modes. The left figure shows non-arm swinging gait and right shows the natural or unaltered arm swinging gait.

during phone use or carrying groceries causes the arms to become fixed in one position rather than swinging freely. Again, these effects have been studied independently with articles comparing arm swinging and the cost to gait mechanics [6], and the stability in gait [2]. However, these articles did not consider how arm swing symmetry effects a gait symmetry with added physical changes to the lower limbs.

The existing body of literature is extensive and provides a rich understanding of many concepts related to physically altered (weight/leg length) gait and dual task walking. However, there is a lack of research exploring how dual task walking alters the symmetry in physically asymmetric gait, and what effects the relationship of altered physical parameters have on the spatio-temporal aspects of gait. The research gives insight on how a passive, at home, gait rehabilitation training technique can be investigated and developed. The following chapters of this thesis present methods and results of the induced symmetry within rotating systems and human gait, and how they can be applied in the fields of dynamic systems, robotics, and gait rehabilitation.

Chapter 3: Symmetry Matching

This chapter encompasses the dynamic system symmetry of the research. First, a general method of induced symmetry is presented and verified. It is then followed by an extension of this method to include collision events, specifically a compass gait PDW. The work in this chapter can be applied to rehabilitation engineering, and is used as the basis for the proceeding chapter's walking experiment.

3.1 Passive Synchronization of Rotating Systems

This section outlines the equations used to derive the kinematics of a two-dimensional general rotating system essential for our passive synchronization method. Subsequently we will use this generalized model to draw out a method to synchronize two or more dissimilar rotating systems. The only requirements for this passive kinematic synchronization of dissimilar systems are: identical degrees of freedom, initial conditions, and torques applied to the systems. These same requirements are also needed to cause two identical systems to have the same motion.

Portions of this section were published in the journal of Nonlinear Dynamics and Systems Theory [20]. For permission, see appendix A.

3.1.1 General Rotating System Model Description

We begin by deriving the equation of motion for a general rotating system with $\check{n}$ *degrees of freedom* and $\check{m}$ *masses per degree of freedom*. Variable notation m symbolizes each individual mass whereas $\check{m}$ symbolizes the *total number* of masses per rotating member (or link). This generalized model is shown in Figure 3.2a, and can be described using Lagrangian mechanics where the Lagrangian is defined as the difference of kinetic and potential energy. Note that this

following formulation of the generalized equation of motion is not novel, however it is used in the subsequently described kinematic matching technique.

$$L(\theta,\dot{\theta},t) = K(\theta,\dot{\theta},t) - U(\theta,t) \tag{3.1}$$

To find the equation of motion, the Euler-Lagrange expression is applied.

$$\frac{d}{dt}\left(\frac{\partial L(\theta,\dot{\theta},t)}{\partial \dot{\theta}_{1,2\ldots\check{n}}}\right) = \frac{\partial L(\theta,\dot{\theta},t)}{\partial \theta_{1,2\ldots\check{n}}} \tag{3.2}$$

Equation (3.2) produces $\check{n}$ equations for $\check{n}$ degrees of freedom of the system. After differentiating and collecting coefficients, the equations of motion of this general dynamic system is a set of $\check{n}$ number of first order nonlinear ordinary differential equations shown in matrix coefficient form in Equation (3.3).

$$[M]\,\ddot{\Theta} \;+\; [N]\,\dot{\Theta}^2 \;+\; [G] \;=\; [T] \tag{3.3}$$

where the coefficient matrices [M], [N], and [G] are given in Equations (3.10), (3.14), and (3.15), respectively. [M] is the inertia matrix coefficient, [N] is the velocity matrix coefficient, and [G] is the position/gravity coefficient matrix. [T] can represent any applied or non-conservative torque functions applied to the system such as actuator torque, joint friction torque, or air resistance experienced by a swinging member.

$$[M]^{\check{n},\check{n}}_{\text{sym}} = \begin{bmatrix} M_{1,1} & M_{1,2}\cos(\theta_1-\theta_2) & \cdots & M_{1,j}\cos(\theta_1-\theta_j) \\ M_{1,2}\cos(\theta_1-\theta_2) & M_{2,2} & & \vdots \\ \vdots & & \ddots & M_{i-1,j}\cos(\theta_{i-1}-\theta_j) \\ M_{1,j}\cos(\theta_1-\theta_j) & \cdots & & M_{i,i} \end{bmatrix} \tag{3.4}$$

Here, each of the coefficients on the diagonal are given by

$$M_{i,i} = \sum_{p=1}^{\check{m}} l_{i,p}^2 m_{i,p} + l_i^2 \sum_{q=i+1}^{\check{n}} \sum_{p=1}^{\check{m}} m_{q,p} \tag{3.5}$$

and the remaining non-diagonal coefficients are given by

$$M_{i,j} = l_i \left[\sum_{p=1}^{\check{m}} l_{j,p} m_{j,p} + \begin{cases} l_j \sum_{q=j+1}^{\check{n}} \sum_{p=1}^{\check{m}} m_{q,p} & j < \check{n} \\ 0 & j \geq \check{n} \end{cases} \right]. \tag{3.6}$$

The subscripts i and j represent the matrix entry indexes for matrix row and matrix column, respectively.

$$[N]^{\check{n},\check{n}} = \begin{bmatrix} 0 & M_{1,2}\sin(\theta_1 - \theta_2) & \cdots & M_{1,j}\sin(\theta_1 - \theta_j) \\ -M_{1,2}\sin(\theta_1 - \theta_2) & 0 & & \vdots \\ \vdots & & \ddots & M_{i-1,j}\sin(\theta_{i-1} - \theta_j) \\ -M_{1,j}\sin(\theta_1 - \theta_j) & \cdots & & 0 \end{bmatrix} \tag{3.7}$$

$$[G]^{\check{n}} = \begin{bmatrix} \sum_{p=1}^{\check{m}} l_{1,p} m_{1,p} sin(\alpha_{1,p} + \theta_1) + (l_1 \sum_{q=2}^{\check{n}} \sum_{p=1}^{\check{m}} m_{q,p}) sin(\theta_1) \\ \vdots \\ \sum_{p=1}^{\check{m}} l_{i,p} m_{i,p} sin(\alpha_{i,p} + \theta_i) + (l_i \sum_{q=i+1}^{\check{n}} \sum_{p=1}^{\check{m}} m_{q,p}) sin(\theta_i) \\ \vdots \\ \sum_{p=1}^{\check{m}} l_{\check{n},p} m_{\check{n},p} sin(\theta_{\check{n},p} + \theta_{\check{n}}) \end{bmatrix} g \tag{3.8}$$

These are the coefficient matrices for the equations of motion of a general rotating system model with $\check{n}$ degrees of freedom and $\check{m}$ masses per degree of freedom. The [M] matrix is a symmetric matrix, while the [N] matrix is a negatively mirrored matrix with a zero diagonal. Note

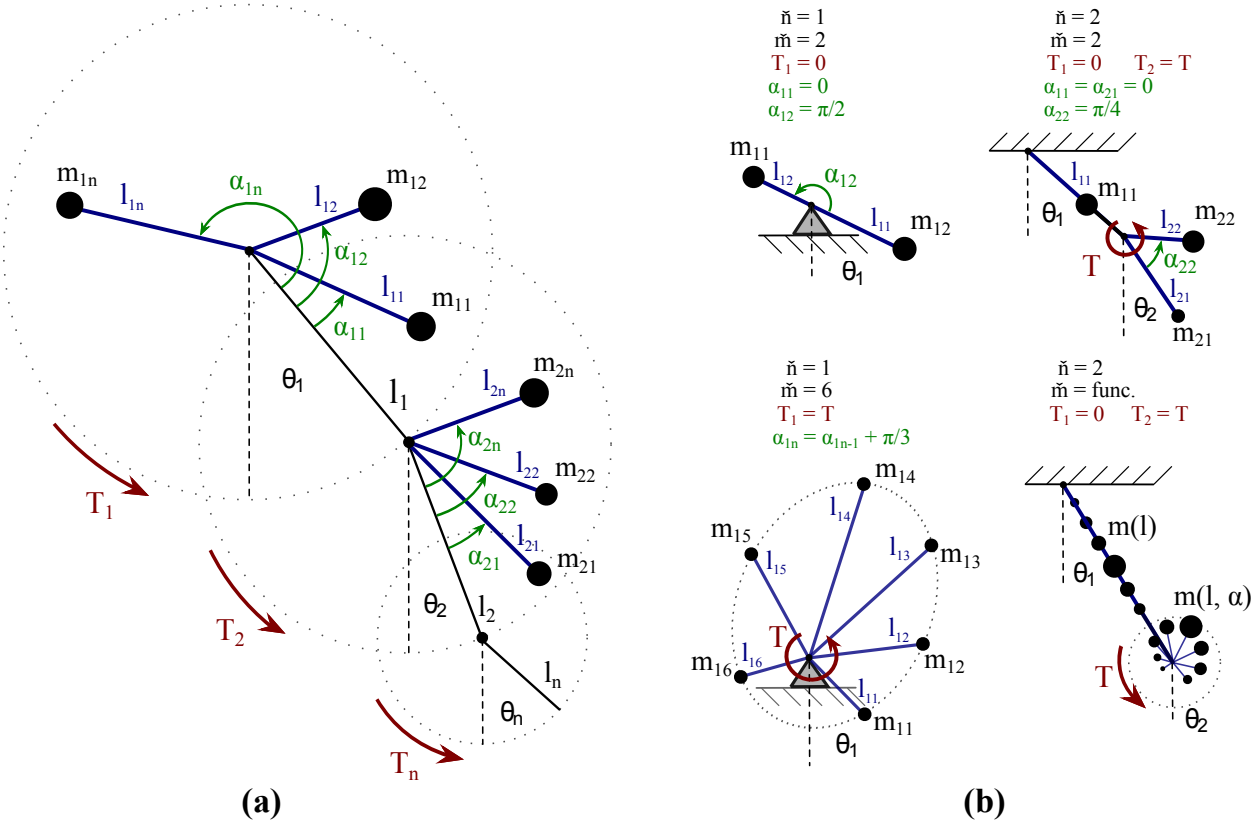

Figure 3.1: Different configurations illustrating the application of the general method. a) Kinematic chain for an $\check{n}$ degree of freedom system with $\check{m}$ masses per link. b) Modified models that can be created using the general synchronization method.

that the coefficients [Equations (3.5) and (3.6)] are all unique matrix components in the $[N]$ matrix that all appear in the $[M]$ matrix. Also note that the last row of $[G]$ ($i = \check{n}$) is different since there are no masses from links further down the kinematic chain sequence. Masses (m) and mass distributions (l) are shown in Figure 3.2a.

Equation (3.3) can model any degree of rotating system or rotating system links. Degrees of freedom (links), mass, and mass distribution within each link can be easily modified to create models for such systems as shown in Figure 3.2b. These modified models can represent rotors, pendulums, cams, or rotating kinematic systems and open kinematic chains.

3.1.2 Passive Kinematic Synchronization using Matched Coefficients

Now that the general point-mass model for a rotational open-ended swinging system has been defined, I am able to utilize the model to create synchronized motion between two dissimilar systems.

Given the same torque input and initial conditions, two or more systems with the same degrees of freedom will exactly match in dynamics if all four coefficient matrices, $[M]$, $[N]$, $[G]$, and $[T]$ in Equation (3.3) are matched between the systems. Since only the computed end values of these coefficients determine the dynamic behavior of the rotating systems, the masses and mass distribution do not have to match between them. This allows for two or more systems with dissimilar mass and mass distribution parameters to kinematically behave identically, that is, have identical dynamic coefficients $[M]$, $[N]$, $[G]$, and $[T]$. For instance, assuming identical torque input and initial conditions, a swinging single link pendulum with two masses can be designed to swing identically to another single link pendulum with two or more masses, where the masses are are distributed differently along the pendulum link. This concept allows for the first and second moments of inertia to be decoupled and greater design flexibility is obtained. Given that each link has two or more masses distributed along the link ($\check{m} \geq 2$), there are infinite combinations of kinetmatically matched systems, that is, there are an infinite number of ways the masses can be distributed such that the four coefficient matrices in Equation (3.3) match another system.

When the coefficient matrices are generalized for systems with $\check{n}$ degrees of freedom with $\check{m}$ masses per link (Equations 3.10, 3.14, and 3.15), a pattern of repeating matrix entries emerges.

Table 3.1: Number of KMCs for any $\check{n}$ degree of freedom system

DOF ($\check{n}$)	Number of KMCs
1	2
2	5
3	9
$\vdots$	$\vdots$
$\check{n}$	$KMC_{\check{n}-1} + (\check{n}+1)$

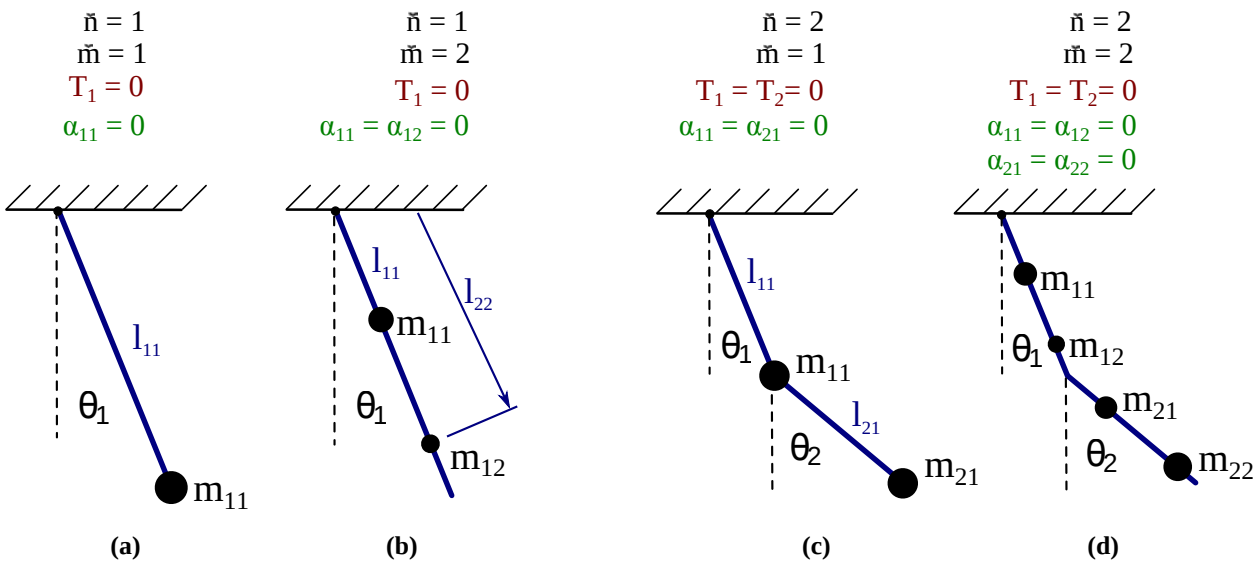

Figure 3.2: Single link and double (2-link) pendulum representation model. (a), (b), and (d) were used experimentally.

It is seen that for the coefficient matrices to match between two rotating systems and cause synchronized dynamics, only unique parts of the coefficient matrices need to be matched between systems. The naming of each unique term that appears in the coefficient matrices will now be called a *kinematically matched coefficient* (KMC). The KMCs are represented in Equations (3.5), (3.6), and (3.15). The total number of KMCs that have to be matched between kinematically synchronized systems is given in Table 3.1. For example, to synchronize the dynamics of a pair of one degree of freedom rotating system, two KMCs need to be matched, while for a pair of three degree of freedom systems to be synchronized, nine KMCs need to be matched.

In the following sections I will present two examples of this matching technique for one and two degree-of-freedom systems with experimental validation.

3.1.3 Example 1: Passive Single Link Pendulum

This section utilizes the method presented in Section 3.1 and experimentally demonstrate its validity. I start with creating two matched variations of a simple passive ($[T] = 0$) single mass (m̌=1) single link (ň=1) pendulum that is shown in Figures 3.2a. The physically asymmetric version of the single link pendulum has two masses per link (m̌=2) (Figure 3.2b).

Although more masses could be utilized to match the motion of this single link pendulum, two masses are sufficient to describe any number of masses and mass distributions. The parameters of all three dissimilar single link pendulums are shown in Table 3.2. Since a single link pendulum is one degree of freedom, only two KMCs had to be matched between systems ($M_{1,1}$=33,600 g-cm^2 and G_1=1,260 g-cm).

3.1.3.1 Experiment Description

The three dissimilar single link pendulum systems were constructed from rigid foam board that was light (1.125g per link) relative to the entire pendulum. Mass and mass distributions were calculated using KMCs in Equation 3.10, 3.14, and 3.15. Lead weights were used as pendulum masses and attached to the link at appropriate positions. The mass values listed in Table 3.2 were rounded to whole grams for the experimental pendulums. To ensure precise link dimensions, each pendulum was cut with a 60W laser cutter (Universal Systems VLS4.60).

The links were attached to a short and rigid 0.375in (0.9525cm) aluminum rod using a precision steel ball bearing to reduce friction. To minimize variability due to friction (negative torque), the exact same bearing was used for each system. Each pendulum system was dropped from the same initial position with an adjustable spring loaded release mechanism. This complete setup can be seen in Figure 3.3.

The pendulums were video recorded at 50 frames/second (50 Hertz) using a Cannon® T3i digital camera with a Cannon® EF 50mm f/1.8 II lens. Link angular position was interpreted with Matlab®, which was used to load video frames and identify each link's distinct color while in motion.

3.1.3.2 Results

Five videos of each pendulum were recorded (15 total). The recorded angular position was averaged and filtered using a low pass 2nd order Butterworth filter at 6 Hz. This angular position data is presented in Figure 3.4 and compared with ideal predicted model behavior. Modeled sys-

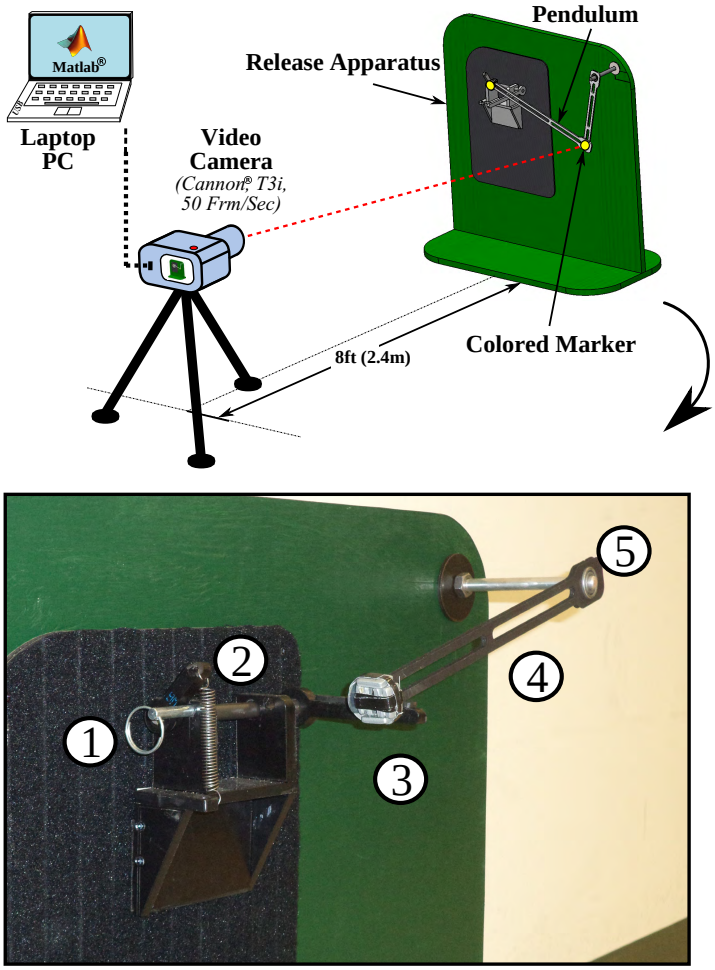

Figure 3.3: Release mechanism used for all pendulum measurements. (1) Release Rod (2) Spring Release Component (3) Weights (4) Foam Pendulum Link (5) Ball Bearing

tems have the same masses and mass distribution as measured physical systems. As predicted, all three ideal modeled systems have the same temporal kinematics and exactly overlap in Figure 3.4. Spectral analysis shows the same frequency peak between all measured physical systems, while all three modeled systems peaked 0.06 Hz below the measured system peaks.

While the recorded physical systems were affected by non-conservative forces, such as air resistance and friction, all three dissimilar pendulums matched kinematically. Their slight difference in amplitude can be explained by the variable mass and mass distribution in the pendulums that leads to variable weight and centripetal forces on the bearing, which in turn increases rotational friction. Similarly, the effect of the friction torque is affected by the inertia of the system. Although the *kinematics* are matched, the *kinetics* in these dissimilar systems does not match; the different

Table 3.2: Single pendulum coefficient equations and experimental parameters

	Coefficient Index	Coefficient Value	System 1 (m̆=1)	System 2 (m̆=2)	System 3 (m̆=2)
KMCs	$\mathbf{M}_{1,1}$	33,600 g-cm^2	$m_{11}l_{11}^2$	$m_{11}l_{11}^2+m_{12}l_{12}^2$	
	$\mathbf{G}_1$	1,260 g-cm	$m_{11}l_{11}$	$m_{11}l_{11}+m_{12}l_{12}$	
Masses (g)			m_{11}=47.3	m_{11}=35.0 m_{12}=21.0	m_{11}=49.0 m_{12}=31.8
Lengths (cm)			l_{11}=26.7	l_{11}=15.0 l_{12}=35.0	l_{11}=5.0 l_{12}=31.9

masses will generate different forces. Despite these small effects, all three physically dissimilar pendulums had a frequency of 0.88 ± 0.04 Hz.

When comparing the collected and model data, the effects of damping become distinct. As a result, the amplitude and period decrease over time for the actual systems as shown in Figure 3.4. As previously explained, the model derivation did not include a damping coefficient, thus its effects on motion was not predicted. Despite this difference, the model and all three physically dissimilar pendulums have very similar motion.

3.1.4 Example 2: Passive Double (Two-Link) Pendulum

The induced symmetry is further investigated by passively synchronizing two ($[T] = 0$) dissimilar double pendulum(ň=2) systems with two masses per link (m̆=2). This rotating model is illustrated in Figure 3.2c and 3.2d and KMCs are shown in Table 3.3.

Traditionally the double pendulum is modeled in Figure 3.2c, however this model is impractical from a design perspective considering that the pivot point between the upper and lower link is exactly where the mass is placed and the link is massless. Hence, for this comparison, I added two masses per link.

3.1.4.1 Experiment Description

Two double pendulums were created using the same fabrication technique and material as the single pendulum experiment in Section 3.1.3. An additional small ball bearing was placed at the pivot point between the upper and lower link with a 0.25in (6.25mm) wooden pin. Both small bearing and pin had a combined weight less than 2 grams.

The links were attached to the same aluminum rod, ball bearing, and were released with the same release mechanism shown in Figure 3.3. Specific colors were placed on each link to track their angular positions. Due to greater acceleration of links, the double pendulum nonlinear motion was again recorded at 50 frames/second with the same camera.

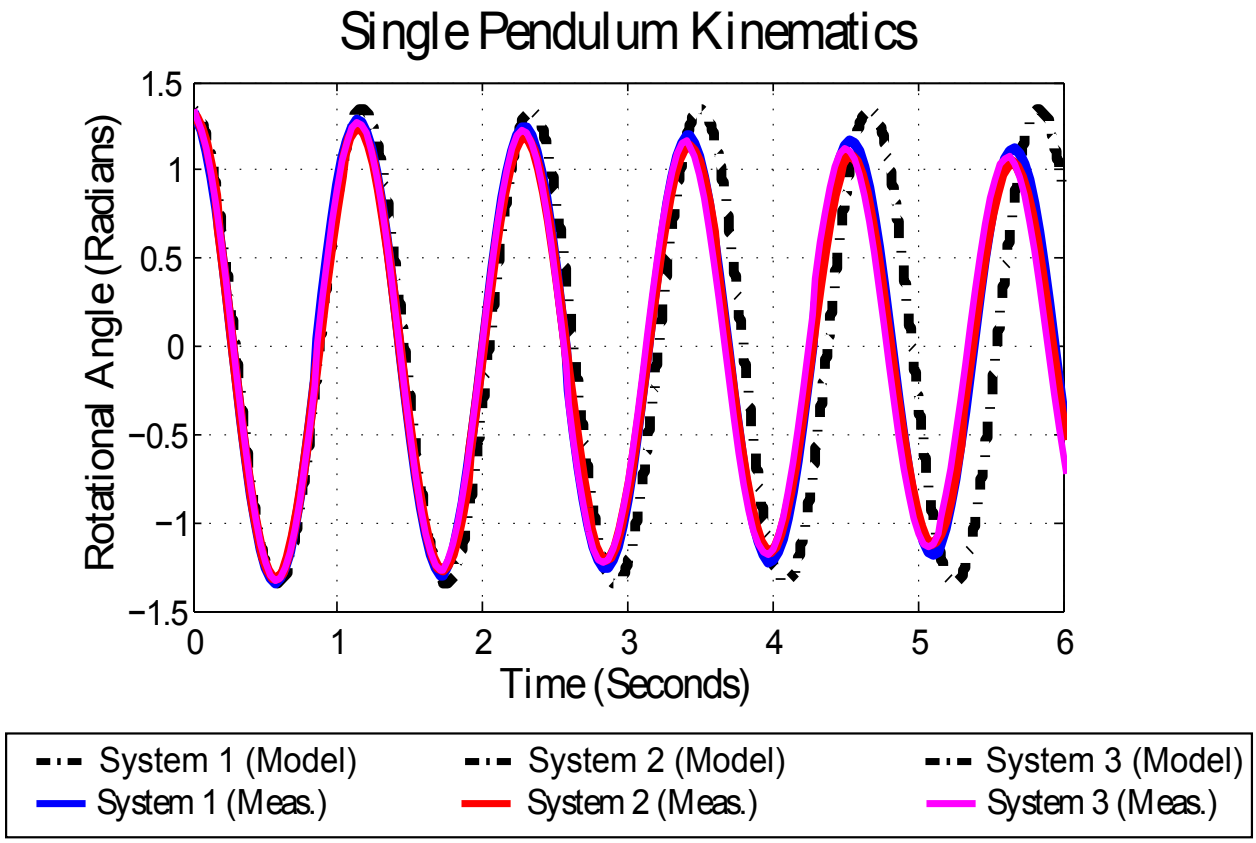

Figure 3.4: The motion of three kinematically synchronized single link pendulums. The motion of the dissimilar modeled systems (dashed line) is matched exactly and overlaps while the measured motion of the three physical system is matched as well. The discrepancy of the modeled and physical system is due to non-conservative forces.

Table 3.3: Double pendulum coefficient equations and experimental parameters

	Coefficient Index	Coefficient Value	System 1 (ǐ=2)	System 2 (ǐ=2)
KMCs	$\mathbf{M}_{1,1}$	28,175 g-cm^2	$l_{11}^2 m_{11} + l_{12}^2 m_{12} + l_1^2 (m_{21} + m_{22})$	
	$\mathbf{M}_{1,2}$	23,800 g-cm^2	$l_1 (l_{21} m_{21} + l_{22} m_{22})$	
	$\mathbf{M}_{2,2}$	32,900 g-cm^2	$l_{21}^2 m_{21} + l_{22}^2 m_{22}$	
	$\mathbf{G}_1$	1,715 g-cm	$l_{11} m_{11} + l_{12} m_{12} + l_1 (m_{21} + m_{22})$	
	$\mathbf{G}_2$	1,190 g-cm	$l_{21} m_{21} + l_{22} m_{22}$	
Masses (g)			m_{11}= 5.0	m_{11}=52.6
			m_{12}=35.0	m_{12}=29.1
			m_{21}=14.0	m_{21}=23.0
			m_{22}=35.0	m_{22}=28.0
Lengths (cm)			l_1=20.0	l_1=20.0
			l_{11}=7.0	l_{11}=5.0
			l_{12}=14.0	l_{12}=15.0
			l_{21}=10.0	l_{21}=12.4
			l_{22}=30.0	l_{22}=32.4

3.1.4.2 Results

As before, each pendulum's angular kinematics were recorded five times (10 total), averaged, and filtered with a 2nd order Butterworth filter at 6 Hz. The results of these angular positions are illustrated in Figure 3.5 and compared with the ideal predicted systems.

The motion for both link 1 (upper link) and link 2 (lower link) was in agreement with model conditions through around 4 seconds, but were in good agreement between experimental measurements throughout the whole trial, which was 12 seconds. This movement of the two systems can be seen in Figure 3.6. All collected data deviates less for link 1 than link 2, which can be explained by the more chaotic movement of the lower link and also because of more variability due to friction in the additional middle pivot.

Even with the frictional and damping forces that were present in the physical verification, its still is able to demonstrate that two dissimilar chaotic systems can achieve the same motion by kinematically matching the two systems. The method can be improved with some considerations

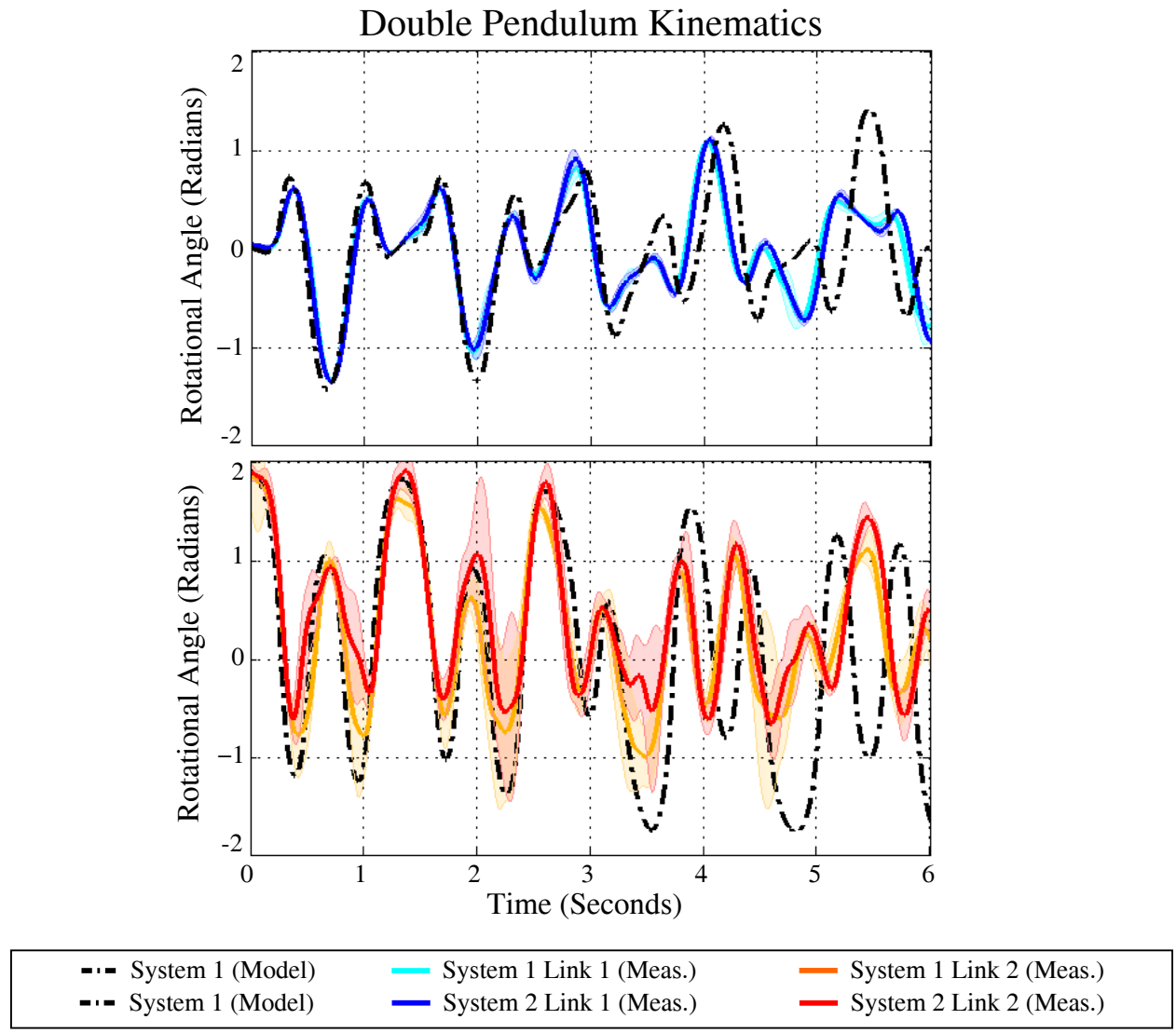

Figure 3.5: Comparison of double pendulum model and experimental results. Shows the rotational link position analysis.

and modeling of external forces. To enhance this method, I will now look at inducing symmetry between two physically asymmetric systems that both experience an external collision.

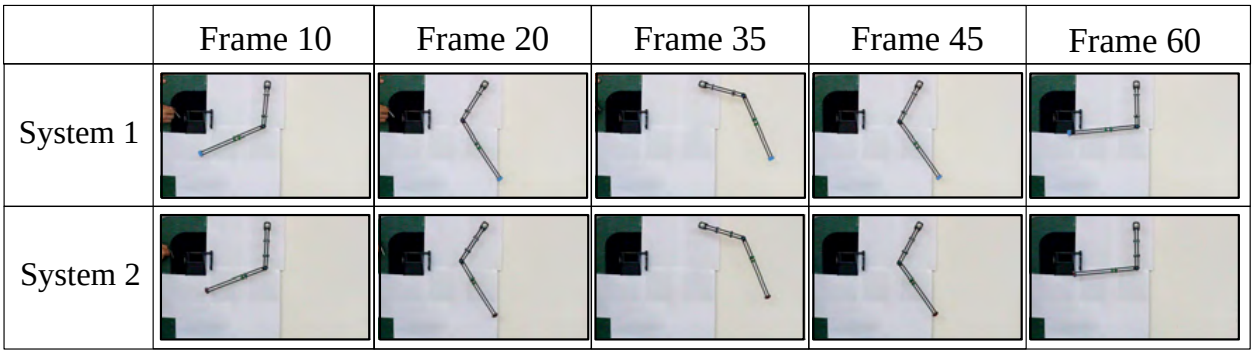

Figure 3.6: Motion of two kinematically synchronized double link pendulums.

3.2 Passive Synchronization of Dynamic Systems with External Collisions

Balancing an asymmetric gait begins with understanding how the underlying dynamics govern or influence its motion. This section will expand on the methods presented earlier in the chapter and will attempt to induce symmetry in dissimilar rotating systems that experience an external collision. A new set of KMCs that define the effect of heel strike in simple walker models will be investigated and applied to solve for symmetry in two asymmetric PDWs. Insight on such systems can provide better models to more accurately predict and understand the behavior of human gait, while also showing what limitations are involved in human testing. These systems can also be useful in the fields of manufacturing, robotics, and especially rehabilitation engineering.

3.2.1 Methods

The external collisions considered in this section are applied to the ends of two inverted double link pendulum systems (commonly referred to as a compass gait model) similar to the one presented in section 3.1.4, and as shown in Figure 3.7c. The free swinging motion of these systems is derived using the Lagrangian method presented in the previous section with an additional number of equations that account for the collision applied.

These collision events, or heel strikes, are considered inelastic in order to better represent the impacts that occur during walking and other practical scenarios. The collisions are also considered instantaneous on a non-slipping surface with no variable friction (i.e. infinite friction).

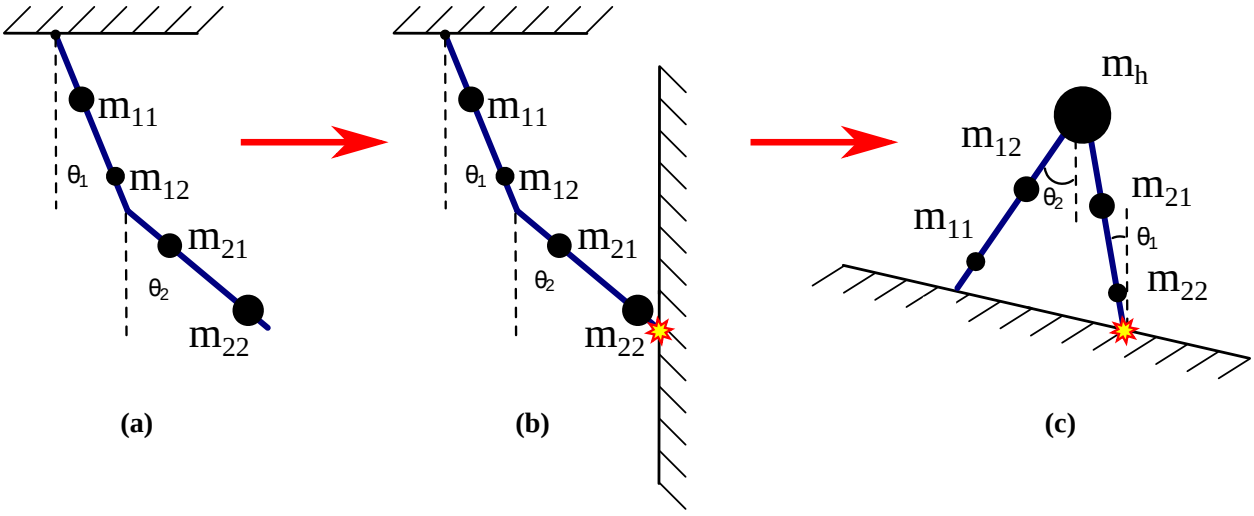

Figure 3.7: The evolution of the KMC matching study. It begins with matching the motion of free swinging systems, but is later adapted to systems that undergo an external collision

3.2.1.1 Free-Swinging Motion

We begin with using the same Lagrangian technique from the previous section to derive the uninhibited swinging motion of these two-link walkers. Equation 3.9 shows the standard form of the planar dynamics.

$$M[\theta]\ddot{\theta} + N[\theta,\dot{\theta}]\dot{\theta} + G[\theta] = T = 0 \tag{3.9}$$

The coefficients that are present in these matrices are what govern the motion of this system. The KMCs are developed by gathering the terms that are repeated, and then grouping them together. This simplifies any dynamics computation and allows us to later match two dissimilar systems. The full derivation of the KMCs of this particular system are shown in Appendix B. After finding the corresponding KMCs we can evaluate each specific coefficient that is present in the M, G, and N matrices.

$$[M]^{\check{2},\check{2}}_{\text{sym}} = \begin{bmatrix} a & b\cos(\theta_1-\theta_2) \\ b\cos(\theta_1-\theta_2) & c \end{bmatrix} \tag{3.10}$$

The coefficients (KMCs) a, b, and c are shown in 3.11 - 3.13.

$$a = m_{22}(L_{21})^2 \; + \; m_{21}(L_{22})^2 \; + \; LL^2(mh + m_{12} + m_{11}) \tag{3.11}$$

$$b = -LL((LR - L_{12})m_{12} + m_{11}(LR - L_{11})) \tag{3.12}$$

$$c = m_{12}(LR - L_{12})^2 + m_{11}(LR - L_{11})^2 \tag{3.13}$$

The N matrix is not necessary when matching two walkers because it consists of the same KMCs that are shown in the previous matrix. However, for clarity and consistency, it is presented below.

$$[N]^{\check{2},\check{2}} = \begin{bmatrix} 0 & b\sin(\theta_1 - \theta_2) \\ -b\sin(\theta_1 - \theta_2) & 0 \end{bmatrix} \tag{3.14}$$

The gravity matrix, G, is the last component needed to identify the free swinging motion of a compass gait PDW.

$$[G]^{\check{2},\check{2}} = \begin{bmatrix} d\sin(\theta_1)gravity \\ e\sin(\theta_1)gravity \end{bmatrix} \tag{3.15}$$

where,

$$d = m_{22}(L_{21}) \; + \; m_{21}(L_{22}) \; + \; LL(mh + m_{12} + m_{11}) \tag{3.16}$$

$$e = m_{12}(LR - L_{12}) + m_{11}(LR - L_{11}) \tag{3.17}$$

The M, N, and G matrices describe the swinging motion of systems that are not under any external torques or forces, other than gravity.

However, in order to simulate an external collision, velocities before and after impact need to be calculated using the conservation of angular momentum. The pre-collision velocity values are easily extracted from the freely swinging system just before impact. The post-collision velocity of each link is calculated by applying the law of conservation of angular momentum for the entire system about the origin, and for the second link rotating about the first. The equations for conservation of angular momentum for a double link pendulum are shown in 3.18.

$$\vec{L}_{11} \text{ x } v_{m_{11}}{}^{pre} \;+\; \vec{L}_{12} \text{ x } v_{m_{12}}{}^{pre} \;+\; \ldots\; \vec{L}_{\check{n},\check{m}} \text{ x } v_{m_{\check{n},\check{m}}}{}^{pre} \tag{3.18}$$

$\vec{L}_{11}$ represents the distance from the rotating origin point to the the corresponding mass, m_{11} shown in 3.8. The same cross product is applied for all the masses in the system. The resulting pre-collision equations are then set equal to the post-collision equations, shown in 3.19.

$$\vec{L}_{11} \text{ x } v_{m_{11}}{}^{post} \;+\; \vec{L}_{12} \text{ x } v_{m_{12}}{}^{post} \;+\; \ldots\; \vec{L}_{\check{n},\check{m}} \text{ x } v_{m_{\check{n},\check{m}}}{}^{post} \tag{3.19}$$

This particular PDW model contains two joint angles, thus two equations are formed for both the pre-collision and post-collision effect, resulting in a 2x2 matrix. These matrices are shown in B.1.

$$Q_{pre}\dot{\theta}_{pre} = Q_{post}\dot{\theta}_{post} \tag{3.20}$$

where,

$$[Q_{pre}]_{\text{sym}}^{\check{2},\check{2}} = \begin{bmatrix} f\,cos(\theta_1 - \theta_2) + g & h \\ g & 0 \end{bmatrix} \tag{3.21}$$

$$[Q_{post}]^{\check{2},\check{2}}_{\text{sym}} = \begin{bmatrix} j + k\,cos(\theta_1 - \theta_2) & i + k\,cos(\theta_1 - \theta_2) \\ j & k\,cos(\theta_1 - \theta_2) \end{bmatrix} \tag{3.22}$$

The KMCs that are present within the collision matrices are shown in equations B.4-B.9.

$$f = LLm_{22}(L_{11}) \; + \; m_{21}LR(L_{22}) \; + \; LLm_{12}(L_{12}) \; + \; LL\,LRm_h \; + \; m_{22}LR(L_{21}) \tag{3.23}$$

$$g = -m_{21}(LL - L_{21})(L_{21}) \; - \; m_{22}(LL - L_{22})(L_{21}) \tag{3.24}$$

$$h = -(LR - L_{12})m_{12}(L_{12}) \; - \; m_{11}(LR - L_{11})(L_{11}) \tag{3.25}$$

$$j = (LL - L_{21})^2 m_{21} + (LL - L_{22})^2 m_{22} + 2(LL - L_{21})(LL - L_{22})m_{22} \tag{3.26}$$

$$k = -LR((LL - L_{21})(m_{21} + m_{22}) + (LL - L_{22})m_{22}) \tag{3.27}$$

$$i = m_{11}(L_{11})^2 \; + \; m_{12}(L_{12})^2 \; + \; LR^2 mh + LR^2 m_{22} + LR^2 m_{21} \tag{3.28}$$

It is important to note that no moments are created from the resulting collision forces, thus no additional torques are applied to the system.

Now we can examine the KMCs of one system and compare them to another in order to solve for symmetry. The complete list of KMCs needed to match any two link walkers with two masses per link and a hip mass are shown in table 3.4. With these KMCs, I can now calculate the motion of two systems that have physically asymmetric masses and mass distributions and

Table 3.4: Complete list of KMCs to match PDW models. These equations are used to match any dissimilar compass gait PDWs that have the same angular dynamics and no torque applied.

Coefficient Index	Corresponding KMC(s)
$M_{1,1}$	a
$M_{1,2}$	$b\cos(\theta_1-\theta_2)$
$M_{2,1}$	$b\cos(\theta_1-\theta_2)$
G_1	$d\sin(\theta_1)gravitiy$
G_2	$e\sin(\theta_1)gravitiy$
$Q_{pre}1,1$	$f\cos(\theta_1-\theta_2)+g$
$Q_{pre}1,2$	h
$Q_{pre}2,1$	g
$Q_{post}1,1$	$j+k\cos(\theta_1-\theta_2)$
$Q_{post}1,2$	$i+k\cos(\theta_1-\theta_2)$
$Q_{post}2,1$	$j+k\cos(\theta_1-\theta_2)$
$Q_{post}2,2$	$k\cos(\theta_1-\theta_2)$

induce symmetry, or synchronize them. Note, similar to the previous section, only the computed end values of these collision and free swinging coefficients determine the dynamic behavior of the rotating systems.

The following section will present the verification of the KMC matching technique for two dissimilar PDW models. The approximate physical asymmetry is illustrated in Figure 3.8.

3.2.2 Simulation Set-Up

To verify the KMCs presented earlier, two physically asymmetric inverted double pendulum systems were evaluated using two methods; analytical and numerical. The asymmetry was applied by changing the values of certain masses between systems and then allowing the remaining variables to be solved. In order to be able to solve such a complex set of equations, several combinations of equations were attempted with a different number of masses on each link, mass values, and link lengths. A base system (Figure 3.8a) was chosen and compared to a different, physically asymmetric system (Figure 3.8b). The goal was to show that both systems can behave identically by matching their KMC values. The asymmetry was induced by assigning different

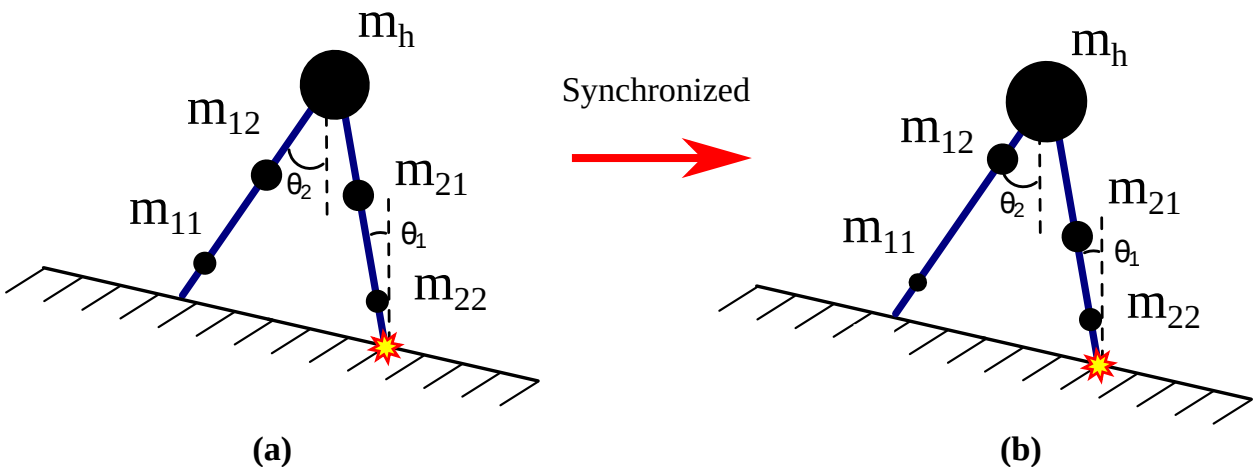

Figure 3.8: Physical illustration of two semi-synchronized PDW compass gait models. (a) Is the given system that we are using to set the KMC values. (b) The hip mass (m_h) and left thigh mass (m_{12}) are specifically increased and some distances are changed along the limbs.

parameter values for certain masses and mass distributions. An explicit solution was attempted with the remaining unknown variables using the eleven KMC equations. Several different equation configurations and variables were explicitly solved for using this method.

The numerical approach for this study was a brute force method that is commonly used in computer science and numerical methods. The brute force calculation evaluates a large number of combinations including values for mass, mass distribution, and link length. System 1 in this calculation is arbitrarily chosen and the KMCs are calculated based on the physical attributes. In order to find a viable match, several physical combinations were calculated. These different combinations were then compared to the model system with a specified threshold, and if the calculated system was below this threshold, it was included as a possible match.

To compare the results of these methods, a simulation was created to show the difference in motion of both systems, similar to those in the previous sections. Average step length data, for left and right step, was collected throughout the simulations and compared after ten steps. The asymmetry, calculated using Equation 3.29, showed the percent difference in the spatial data of the systems.

$$PercentAsymmetry = \frac{(L_{step} - R_{step})}{((L_{step} + R_{step})0.5)} \tag{3.29}$$

In addition, the joint angles were compared and analyzed for both left and right step. All final data was calculated, simulated, and analyzed using Matlab®.

3.2.3 Results

The analytical approach to this study was unable to find any matching system. As stated earlier, several different equation configurations were used and all platforms used to solve these equations, including Mathematica®, Mathcad®, and Matlab®, resulted in similar failure. Even the variables being solved were changed, but still no matching motion could be achieved between these systems. This might have been due to the complexity of the equations or the difficult computation involved. This may also suggest a complete match is not feasible with collision equations or any walking models.

The numerical brute force method, however, did result is successful matches below a six percent threshold as shown in Figure 3.9. Hundreds of successful semi-symmetric systems were found, but not all were able to show a consistent and stable gait pattern. The systems that did show stable gait were compared to the base system in terms of spatial parameters, and joint angles.

The step length asymmetry after ten steps was calculated for both the left and right step, using equation 3.29. The left step length was only 2.5 percent different between the two systems, while the right step showed a 9.6 percent asymmetry, as shown in Table 3.5. Although this seems high for a walking model, this is likely due to the shorter right leg of the matched system.

The joint angle data, however, was very close for all steps as indicated by Figure 3.9 which shows a close match for the duration of the step for both angles. Again, the slight difference in the θ_1 angle might be due to difference in leg length and the angle of the colliding foot changing faster then the base system.

Table 3.5: Results comparing two physically asymmetric PDWs

Comparing Systems	
Left Step Length	**Right Step Length**
2.5%	9.5%

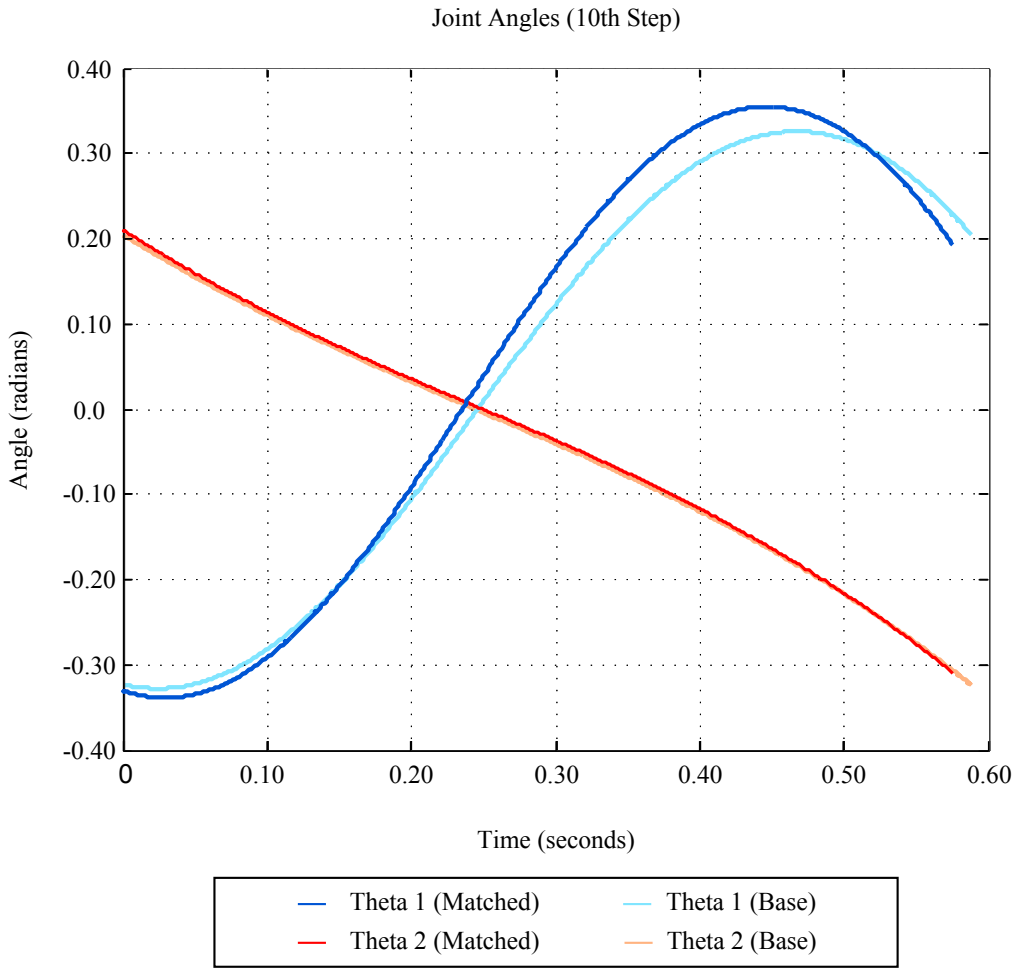

Figure 3.9: Joint angle differences of two dissimilar compass gait models.

Despite the fact that there were semi-symmetric systems found, no completely synchronized systems emerged. Even if longer computations and larger parameters searches are performed, I do not think a perfect match can be achieved in these types of systems. This is most likely due to the force inequalities that occur when two systems do not possess the same kinetic energy because of varying mass values.

Although there was limited success of this method, it can be used to synchronize systems within a certain percentage, which still might have applicable usage in the fields of robotics and rehabilitation engineering. With this result, its clear that the collision symmetry and their KMCs lack the same generalizability as the previous section.

Chapter 4: Walking Symmetry

With the complexity of modeling the human's conscious actions and reactions in gait, I expand the work of the previous chapter and adapt the concept to human walking with some experiments on altering gait patterns. This chapter presents a gait study on the passively induced symmetry of human walking. Here I investigate how changing the physical configurations of two symmetric limbs change the step length, step time, and ground reaction forces. The goals of this chapter are as follows:

1. Find asymmetric physical configurations that can exhibit symmetric behaviors.
2. Investigate the difference in how conscious and subconscious control affects gait with these physical changes.
3. Show how changes in arm swinging influence the gait with different physical limb combinations.

In general, this study can be used to tie together the passive synchronization methods previously discussed and the symmetry, or asymmetry, present in human gait that inherently involves this conscious factor.

4.1 Procedure

A complete outline for the experiments and the setup are presented in this section. Participants in this study were asked to walk for several minutes with different physical configurations, with these including both conscious and distracted sessions.

All the experiments were performed on a Computer Assisted Rehabilitation ENvironment (CAREN) system, shown in Figure 4.1. This system includes a split belt treadmill, two individual

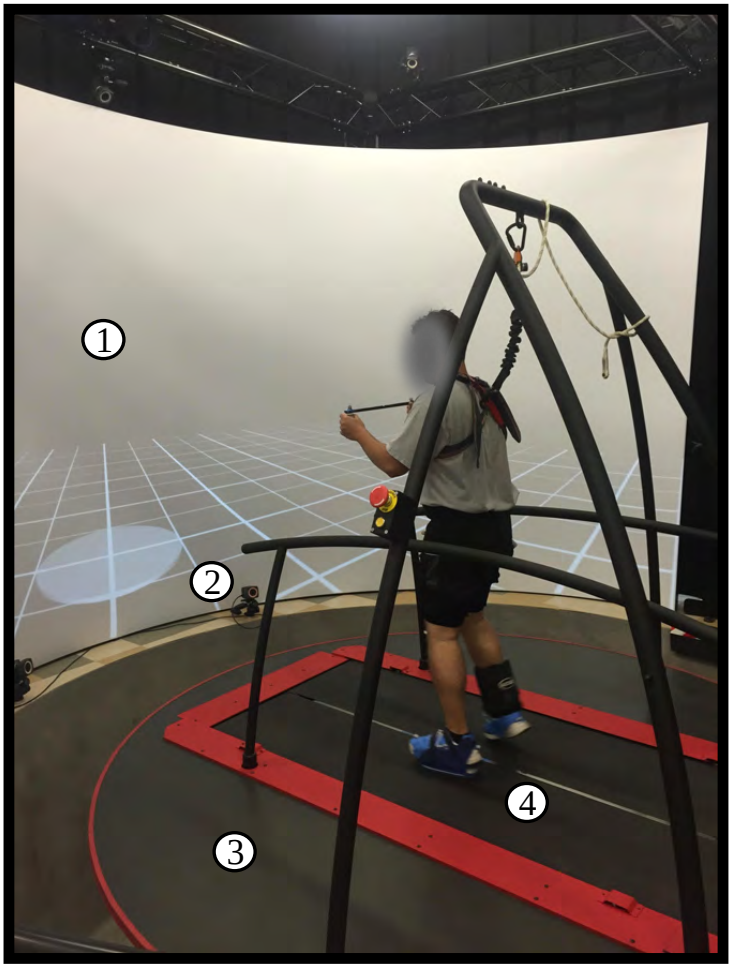

Figure 4.1: An image of the CAREN system and environment. 1) A 180 degree screen projector for virtual environments. 2) Infrared cameras to track marker motion. 3) Six degree of freedom platform. 4) Split belt treadmill and force plates.

force plates, and a six degree of freedom platform. The ground reaction force data was gathered from these force plates for both the left and right leg of each subject. Specifically, this study examines the push-off, vertical, and braking forces.

The split belt treadmill used in this study was set to equal speeds, and was based on the steady state walking (physically unaltered walking) velocity of each participant. The baseline, or steady state walking, was calculated based on an average of three different 10 meter walking tests, where the participant was told to walk at a normal pace.

The CAREN system also includes a motion capture system which provided the spatial data for this study. All the kinematic analysis of all the walking studies was done using a Vicon® infrared camera motion tracking system. This system includes 10 Vicon® bonita B10 cameras that record at 120 Hz. Each participant was equipped with 8 infrared markers (14 mm Diameter), placed on the toe, heel, knee and pelvis for both the left and right sides of the body.

All data was processed using a Matlab® script to calculate average step length, step time, and ground reaction forces. Additional processing was also done in Matlab®, including performing ANOVA statistical analysis, generating data figures, and animations.

4.1.1 Physical Parameters

Each combination of physical parameters was performed once, with the exception of the baseline walking that was performed at the start and end of the experiment. The order of these combinations was randomized for each subject, excluding sessions one, two, and fourteen. For each of the ten different participants tested, the first two sessions were always baseline walking without the distraction device, followed by baseline walking with the device (device explained in section 4.1.2). The last session (fourteen) performed by each participant was an additional baseline study (without device) to evaluate any adaptation that might have developed.

The length of each individual walking session was approximately two minutes, with varying times in between to apply physical alterations. To avoid the effects of adaptation from previous physical combinations in the study, only the last thirty seconds was evaluated in each session. The total walking time for the entire experiment was approximately twenty eight minutes for each subject, and a short break was available to the participants between sessions, but this was not compulsory.

The fourteen different physical combinations of this walking study are shown in Table 4.1. The leg length device was attached to the non-dominant foot of the participant and is shown in Figure 4.3. The two settings for the applied leg length change were small and large, measuring 0.027 meters (1.05 inches) and 0.052 m (2.05 inches) respectively. It was designed to be under

Table 4.1: All combinations of settings that were applied to the participants. Note: combinations 3-13 were randomized for each participant.

Combination	Leg Length Change	Weight Applied	Distraction Device
1	*None*	*None*	*None*
2	*None*	*None*	*Included*
3	*None*	*Small*	*None*
4	*None*	*Large*	*None*
5	*None*	*Large*	*Included*
6	*Small*	*None*	*None*
7	*Small*	*Small*	*None*
8	*Small*	*Large*	*None*
9	*Large*	*None*	*None*
10	*Large*	*None*	*Included*
11	*Large*	*Small*	*None*
12	*Large*	*Large*	*None*
13	*Large*	*Large*	*Included*
14	*None*	*None*	*None*

0.350 kg (0.77 lb) for the high setting and under 110 g (0.25 lb) for the lower setting. These small mass values ensured that this shoe would only simulate pure leg length change and not add unwanted weight. For the application of weighted walking, a weighted ankle strap with several lead weight inserts was attached to the dominant leg. There were two distinct mass values for this parameter, as shown in Figure 4.4. The small weight size was approximately 2.3 kg (5.07 lb), and the large was 4.6 kg (10.14 lb). An additional strap was included as to note interfere with any infrared position sensing markers.

4.1.2 Distraction Device

To test the dual task walking effects of the added physical parameters, a small device was used to distract the participants. This device allows us to test the more passive nature of human walking which was a vital part of this walking study. A passive walk refers to the subconscious state of gait when a subject does not actively think about how they are walking. Inherently, when a subject is asked to participate in a gait study, they are more inclined to think about how their gait is behaving, thus consequently changing the otherwise passive nature of the gait cycle.

Figure 4.2: Illustration of the distraction device that was used in the experiment. Participants were asked to balance the ball in the middle of the device while walking for two minute sessions.

In addition to providing a distraction, the device will allow me to explore the differences in arm swinging and non arm swinging during gait. This portion of the walking study will show how the body uses arm swinging to compensate for changes in physical parameters of the lower limbs, and if arm-swinging improves the gait symmetry.

The device, illustrated in Figure 4.2, requires the subject to balance the small white ball on a half cylinder for the entire duration of the two minute sessions. It was constructed from an 18 inch long (1 inch diameter) PVC pipe and rubber coated to provide a smooth surface for the ball. Two small crutch handles were attached to both ends of the device, providing an ergonomic grip and secure hold during walking.

The distraction device was used in only testing the largest settings for each parameter (i.e. Large Leg Length and/or Large Weight) for a total of four configurations. A short training session was available for each subject to become acquainted with the device while walking simultaneously. To be able to differentiate the data, two additional markers were placed on either end of the device.

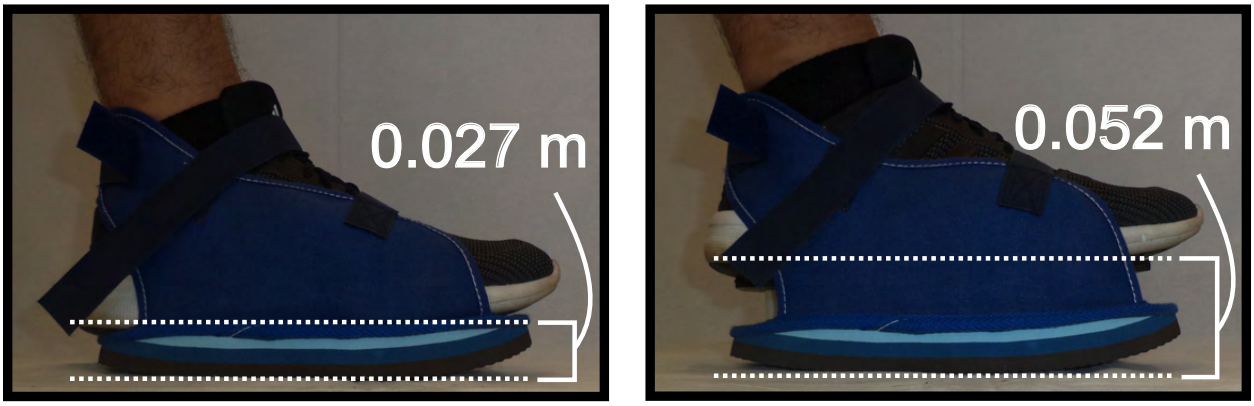

(a) (b)

Figure 4.3: The platform shoe that was used to simulate two leg length increases. (a) Had no additional padding while (b) had a rubber slab with PVC supports to increase height.

Although these markers were not used in the analysis of this experiment, they might be helpful in other studies using this data studying the symmetry of left and right side balance during walking.

4.2 Participants

There were ten subjects (8 male, 2 Female) that participated in the walking study, all with limited to no exposure with physically induced asymmetric walking. The age of the participants ranged from 20 to 30 years old, with no physical impairments, past knee injuries, or large leg length discrepancies. The average height, leg length, weight, and walking speed of the participants was 1.785 m (70.3 in), 0.981 m (38.6 in), 82.8 kg (182.5 lbs), and 1.22 m/s (48.03 in/s), respectively. None of the participants expressed any difficulty performing the walking tasks with or without the distraction device.

Nine of the ten participants in the study were right foot dominant. The data of the left foot dominant subject was mirrored to be included in the analysis. Note, the dominant foot was always used for the applied weight and the leg length change was always applied to the non-dominant foot for consistency. All experiments were conducted with the approval of the Institutional Review Board at the University of South Florida.

(a) (b)

Figure 4.4: The two different ankle weights used in this walking experiment. An additional strap was included for the heavier weight (b)

4.3 Results and Discussion

The distraction device showed minimal effect for spatial and temporal symmetry, as well as vertical and push-off ground reaction forces. It did, however, show a statistical significance for the braking force symmetry ($F(1,125) = 16.52$, $p < 0.0001$). The post hoc analysis showed significant difference in braking force between distracted and conscious walking. This result demonstrates how the distracted gait can not accurately anticipate or mitigate the foot speed or force upon colliding with the floor. It also implies that the human motor control reacts well, subconsciously, to adverse physical changes that might want to induce asymmetry in gait in spatio-temporal parameters. The remaining analyses are for walking without the distraction device.

The lack of differences in the spatio-temporal data with and without arm-swinging might suggest that it does not assist or compensate enough for these physical changes. Without the assistant of arm-swinging, the body most likely uses other techniques to appropriately balance itself, including moving the torso (center of mass) to help ease imbalances due to physical asymmetry.

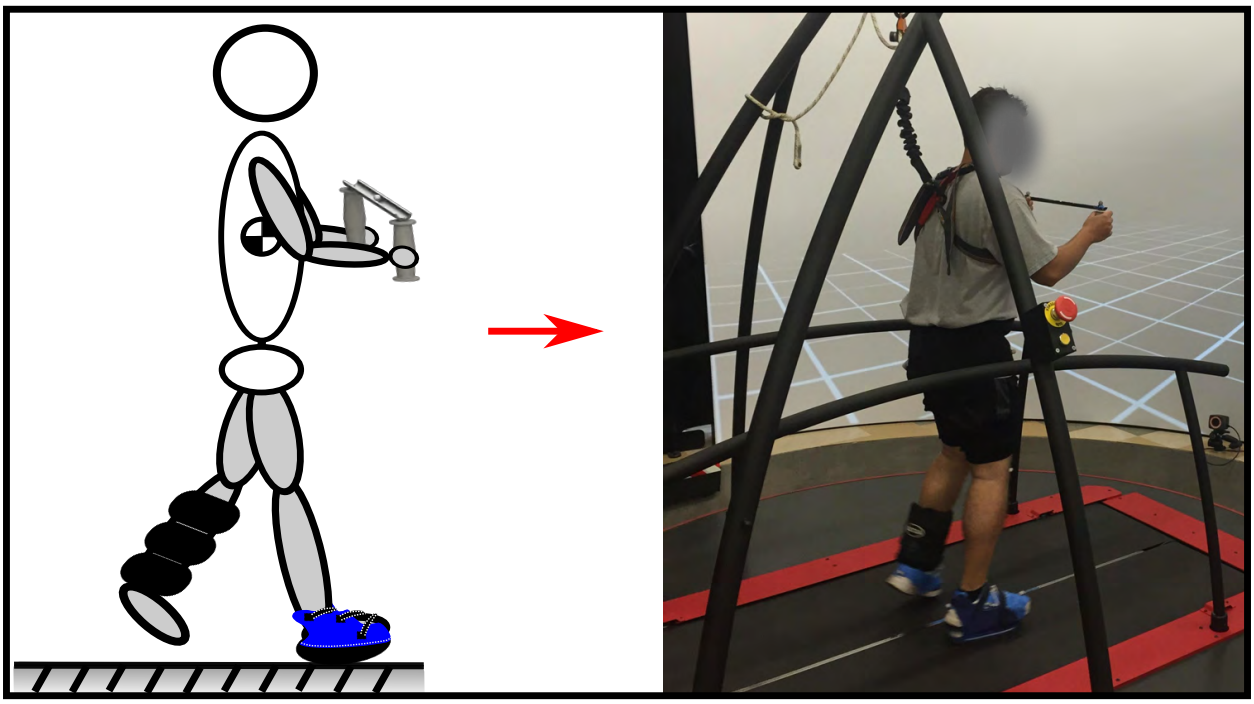

Figure 4.5: The combination of physical parameters and distraction device.

Other significant statistical data was found for differences in vertical and push-off forces. Vertical reaction forces showed a statistically significant difference for leg lengths ($F(2,125) = 111.52$, $p<0.0001$) and weights added ($F(2,125) = 19.15$, $p<0.0001$). A post hoc test for both leg length and weight revealed noticeable differences in both factor levels. Similar results were shown for the push-off reaction, with a statistical significance for leg length ($F(2,125) = 111.52$, $p<0.0001$) and weight ($F(2,125) = 111.52$, $p<0.05$). (All ANOVA and post-hoc results are shown in Appendix C)

The spatial results of the experiments indicated that added leg weight did not noticeably influence the step length symmetry, however it did show an effect of temporal parameters. From the data shown in Figure 4.6, it is clear that the step length for both left and right leg remains unaffected by the added weight. However, the weight did slow down the affected limbs in almost all cases. Perhaps this indicates that because the muscles in the lower limbs are large, they are able to compensate, spatially, for the added weight, while temporally they are impeded. This might

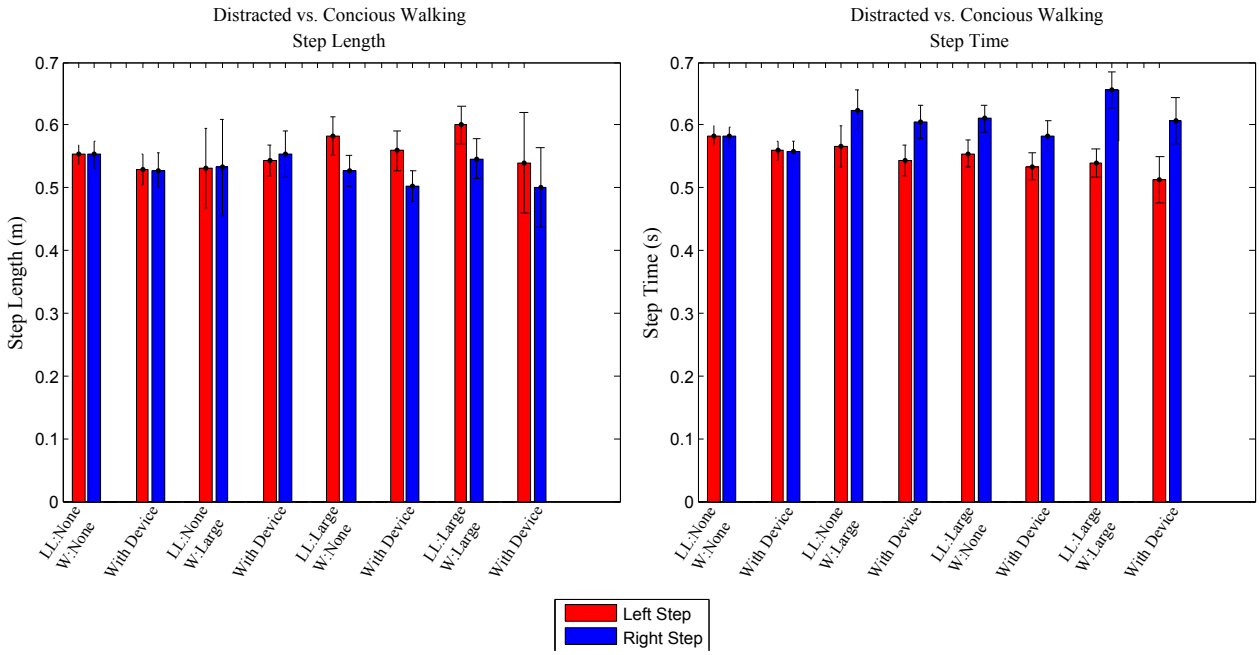

Figure 4.6: Comparison of conscious and subconscious walking. This figure shows the differences in spatio-temporal results.

also suggest that the human legs are able to ignore asymmetrically applied weight and maintain a symmetric step length.

In contrast, added leg length had noticeable effects on both spatial and temporal gait symmetry. For every increase of the leg length parameter both the step length and step time differences increased. These differences, illustrated in Figure 4.7, suggest that having symmetric leg lengths will likely increase the chance for a symmetric gait. This data is in agreement with the previous section, which indicated that even a small difference in leg length (LLD) can cause large percentages of gait asymmetry.

When analyzing the data for configurations of both the physical parameters of leg length and ankle weight together, the effects are amplified. The data shown in Figures 4.7 and 4.8 show that when both are combined at a high setting, the effects are increased dramatically. For instance, the step time of the combined parameters is close to double the value of either parameter individually. This trend is also evident in the ground reaction force symmetry. Further studies are

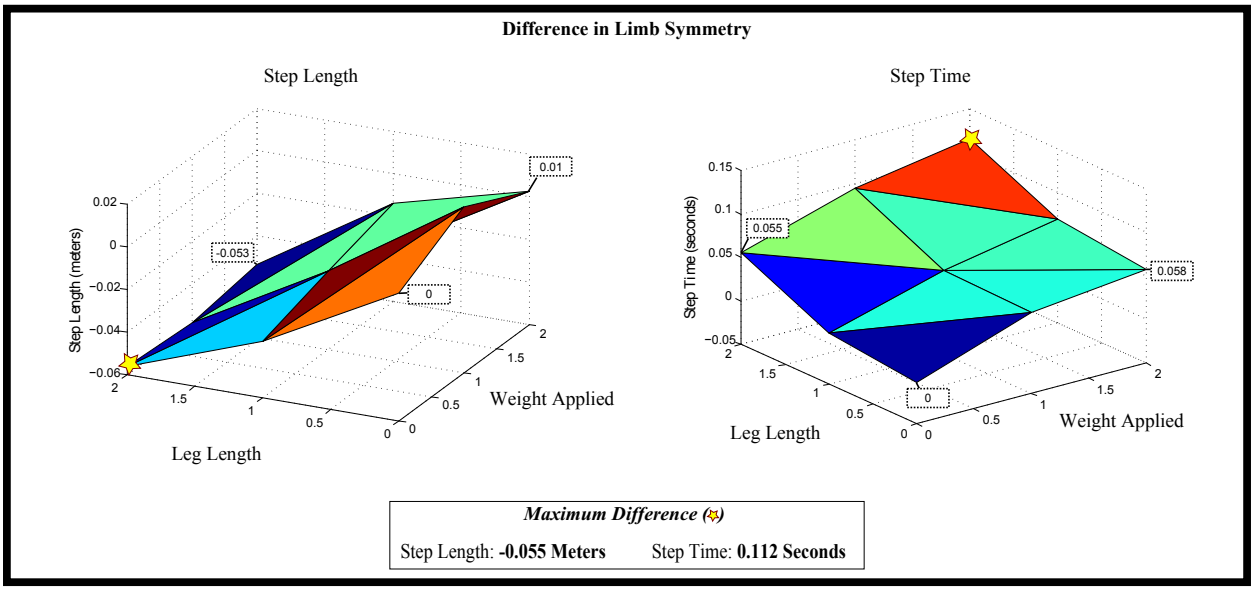

Figure 4.7: Three dimensional figure showing spatio-temporal differences. The x and y axes indicate the physical parameter changes (i.e. 0 is no change and 2 is the large setting).

needed to investigate how the two behave when applied to a single leg, and when the weight is placed in locations other than the ankle.

This research shows that certain physical alterations can affect the spatial and temporal parameters of human gait, which might have implications for gait rehabilitation. For instance, if a patient exhibited asymmetric spatial gait parameters (step length) they might be able to apply a weight of small leg length change to a specific location to bring them closer to symmetry. Even if this does not bring a patient back to complete symmetry, a more symmetric gait might be beneficial in terms of exertion and perception.

Further developments and studies need to be performed in order to investigate how adaptation of these physical changes is retained. If a trend of retention is shown, then people with asymmetric gait might be able to wear a leg lengthening shoe and/or apply a weight to one of their legs to train for improved gait symmetry. This would make rehabilitation significantly easier to perform and financially beneficial to the patient. Future studies might also incorporate the physical changes to just one leg. and how the added effects alter gait symmetry.

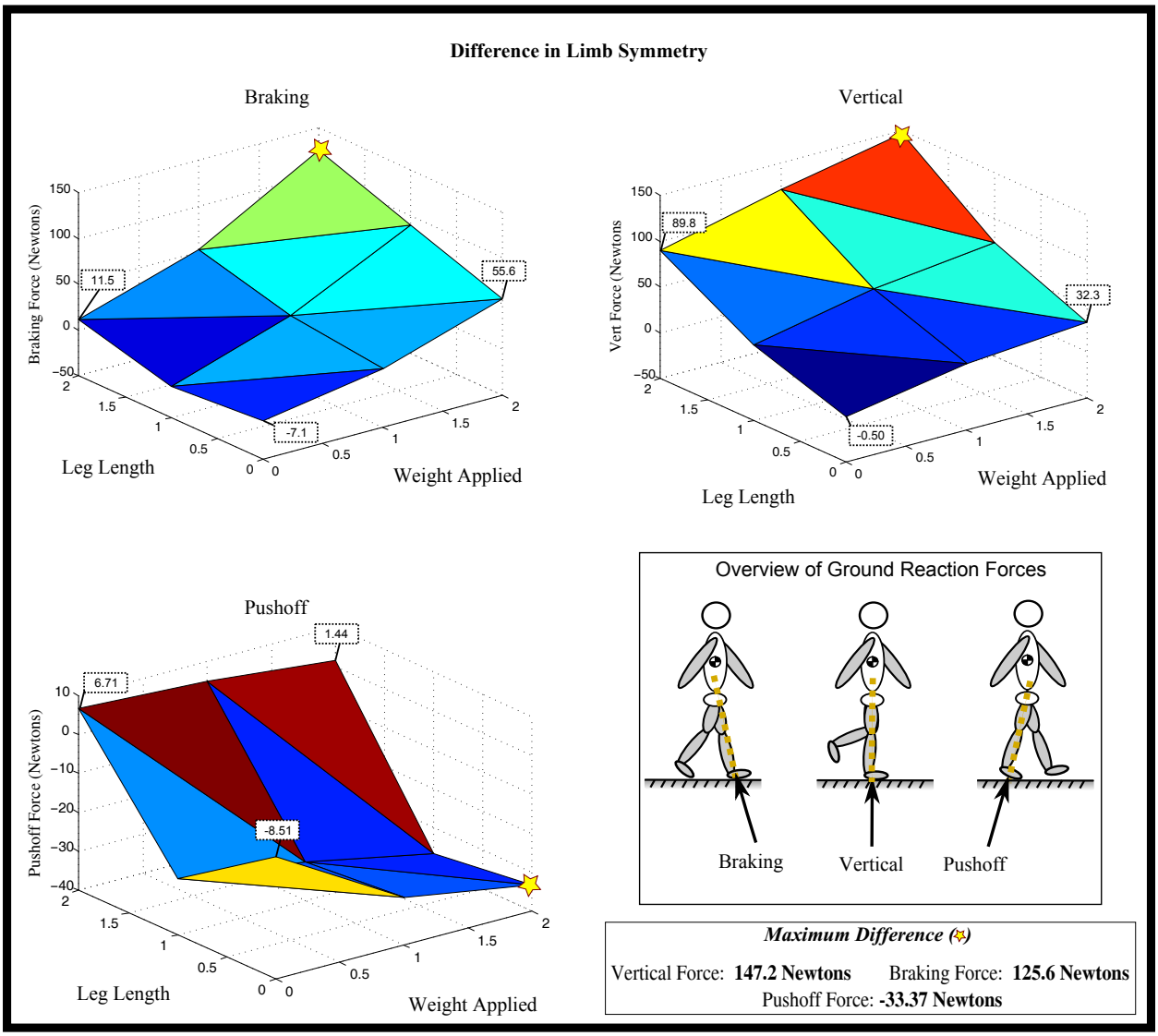

Figure 4.8: Ground reaction force data for all combinations of physical parameters.

Chapter 5: Conclusions

Induced symmetry of kinematics proved to be successful between two rotating dissimilar dynamic systems. Simulating motion without collision events demonstrated that there was no difference in the kinematics for the experiment. Just as the method suggested, the two degree of freedom system (two double-link pendulums) resulted in exact kinematic matches for the entire simulation time because their respective KMCs were equal. This is particularly significant for such a system, as the motion of each link is highly nonlinear. The physical experiment results verified the matched motion with a slight discrepancy that resulted from non-conservative forces such as friction. While we have been able to synchronize dynamics of two uncoupled dissimilar rotating systems over time, it is clear that internal forces, dynamics and time of such a set of systems cannot be synchronized. This is due to the mass values; in order for forces to be the same between two systems, they must have the same mass values at each location. (i.e. the systems would not be dissimilar).

The collision matching experiment showed that only a percentage of kinematic symmetry can be induced between two systems that experience an external collision. This is likely due to the differences in the kinetics (energy) of each system, and as both systems comprise of different mass values, an exact match will never be achieved between two physically asymmetric PDWs. The simplicity of the models in this experiment also suggest that the more complex and realistic the models become, the harder inducing kinematic symmetry will become.

This generalized method shows it is possible to manipulate limb movements by adding or removing masses to key locations along a swinging limb that can assist in balancing out asymmetric walking patterns created by some trauma or neurological disorder. For instance, we can analyze the kinematics between two limbs and improve the intra-limb synchronization with passive means.

The final goal would be the ability to incorporate our results in assisting with designing a prosthetic device best suited for a person's overall gait. This would involve designing a device that requires less energy needed to walk while maintaining a partially synchronized walking pattern.

The walking experiment showed that weight and leg length both influence the gait symmetry in human walking. Distracted and non arm swinging gait did not show any affect to the added physical asymmetry. While spatially and temporally the distracted gait was unaltered, the braking force during distracted walking showed slight differences. This might suggest a loss of heel strike anticipation during dual task walking. Knowing exactly how each of these affect the gait symmetry can have implications for improving and developing new rehabilitation devices. The study also indicates that a person with a physically altered gait can improve their symmetry, but can never achieve a completely symmetric gait.

List of References

[1] E. Begleiter. The effect of the principles of dynamic symmetry on modern art and science. Master's thesis, MASSACHUSETTS INSTITUTE OF TECHNOLOGY, 1984.

[2] S. M. Bruijn, O. G. Meijer, P. J. Beek, and J. H. van DieÃńn. The effects of arm swing on human gait stability. *The Journal of Experimental Biology*, 213:3945–3952, 2010.

[3] D. R. Budney and D. G. Bellow. On the swing mechancis of a matched set of golf clubs. *Research Quarterly for Exercise and Sport*, 53(3):185–192, 1982.

[4] M. Bunnett, M. F. Schatz, H. Rockwood, and K. Wiesenfeld. Huygens's clocks. *Proceedings: Mathematical, Physical and Engineering Sciences*, 458(2019):563–579, March 2002.

[5] V. F. H. Chen. Passive Dynamic Walking with Knees: A Point Foot Model. Master's thesis, Massachusetts Institute of Technology, 2005.

[6] S. H. Collins, P. G. Adamczyk, and A. D. Kuo. Dynamic arm swinging in human walking. *Proceedings of The Royal Society B*, 282, 2009.

[7] L. S. DeBolt and J. A. McCubbin. The effects of home-based resistance exercise on balance, power, and mobility in adults with multiple sclerosis. *Archives of Physical Medicine and Rehabilitation*, 85, 2004.

[8] R. Dilao. Antiphase and in-phase synchronization of nonlinear oscillators: The huygenss clocks system. *Chaos*, 19, June 2009.

[9] G. Ebersbach and M. R. D. W. Poewe. Influence of concurrent tasks on gait: A dual-task approach. *Perceptual and Motor Skills*, 81:107–113, 1995.

[10] J. L. Everett. Dynamical matched set of golf clubs. US Patent. 4,415,156, Oct.17, October 1972.

[11] A. L. Frandkov and B. Andrievsky. Synchronization and phase relations in the motion of two-pendulum system. *International Journal of Non-Linear Mechanics*, 42:895–901, March 2007.

[12] M. Garcia, A. R. Anindya Chatterjee, and M. Coleman. The simplest walking model: Stability, complexity, and scaling. *Journal of Biomechanical Engineering*, 120:281–288, 1998.

[13] H. Geyer, A. Seyfarth, and R. Blickhan. Compliant leg behavior explains basic dynamics of walking and running. *Proceedings of the Royal Scociety*, (273):2861–2867, August 2006.

[14] C. Gibson-Horn. Balance-based torso-weighting in a patient with ataxia and multiple sclerosis: A case report. *Journal of Neurologic Physical Therapy*, 32(3):139–146, 2008.

[15] G. A. Greendale, G. J. Salem, J. T. Young, M. Damesyn, M. Marion, M.-Y. Wang, and D. B. Reuben. A randomized trial of weighted vest use in ambulatory older adults: Strength, performance, and quality of life outcomes. *Journal of the American Geriatrics Society*, 48(3):305–311, 2000.

[16] R. Gregg, Y. Dhaher, A. Degani, and K. Lynch. On the mechanics of functional asymmetry in bipedal walking. *IEEE Transactions on Biomedical Engineering*, 59(5):1310–1318, 2012.

[17] R. D. Gregg, A. Degani, Y. Dhahe, and K. M. Lynch. The basic mechanics of bipedal walking lead to asymmetric behavior. In *Proc. IEEE Int. Conf. Rehabilitation Robotics*, pages 816–821, 2011.

[18] B. Gurney. Leg length discrepancy. *Gait & Posture*, 15(2):195–206, 2002.

[19] I. Handžić, E. Barno, E. V. Vasudevan, and K. B. Reed. Design and pilot study of a gait enhancing mobile shoe. *J. of Behavioral Robotics*, 2(4):193–201, 2011.

[20] I. Handžić, H. Muratagic, and K. B. Reed. Passive kinematic synchronization of dissimilar and uncoupled rotating systems. *Nonlinear Dynamics and Systems Theory*, 2015.

[21] I. Handžić and K. B. Reed. Validation of a passive dynamic walker model for human gait analysis. In *Proc. IEEE Eng. Med. Biol. Soc.*, pages 6945–6948, 2013.

[22] I. Handžić and K. B. Reed. Comparison of the passive dynamics of walking on ground, tied-belt and split-belt treadmills, and via the gait enhancing mobile shoe (GEMS). In *Proc. IEEE Int. Conf. Rehabilitation Robotics*, June 2013.

[23] T. Hatsukari. 3rd Honda ASIMO [online image]. retrieved September 20, 2015 from Wikimedia, December 2007.

[24] J. H. Hollman, F. M. Kovash, J. J. Kubik, and R. A. Linbo. Age-related differences in spatiotemporal markers of gait stability during dual task walking. *Gait & Posture*, 26:113–119, June 2007.

[25] C. Honeycutt, J. Sushko, and K. B. Reed. Asymmetric passive dynamic walker. In *Proc. IEEE Int. Conf. Rehabilitation Robotics*, pages 852–857, June 2011.

[26] F. Iachello. Beauty in nature: Symmetry. volume 1488, pages 402–412. American Institute of Physics, October 2012.

[27] T. P. Jorgensen. Matched set of golf clubs. US Patent. 4,415,156, Nov.15, November 1983.

[28] K. R. Kaufman, L. S. Miller, and D. H. Sutherland. Gait asymmetry in patients with limb-length inequality. *Journal of Pediatric Orthopaedics*, 16(2):144–150, 1996.

[29] A. Khan and P. Tripathi. Synchronization, anti-synchronization and hybrid-synchronization of a double pendulum under the effect of external forces. *International Journal Of Computational Engineering Research*, 3(1):166–176, 2013.

[30] A. Khan and P. Tripathi. Synchronization between a fractional order chaotic system and an integer order chaotic system. *Nonlinear Dynamics and Systems Theory*, 13:425–436, 2013.

[31] A. T. Klimek and A. Klimek. The weighted walking test as an alternative method of assessing aerobic power. *Journal of Sports Sciences*, 2007.

[32] A. D. Kuo. The six determinants of gait and the inverted pendulum analogy: A dynamic walking perspective. *Human Movement Science*, 26:617–656, July 2007.

[33] T. Lam, M. Anderschitz, and V. Dietz. Contribution of feedback and feedforward strategies to locomotor adaptations. *Journal of Neurophysiology*, 95:766–773, 2006.

[34] A. C. Little. Domain specificity in human symmetry preferences: Symmetry is most pleasant when looking at human faces. *Symmetry*, 6:222–233, April 2014.

[35] L. A. Malone and A. J. Bastian. Thinking about walking: Effects of conscious correction versus distraction on locomotor adaptation. *Journal of Neurophysiology*, 103:1954âĂŞ1962, 2010.

[36] J. E. Marsden and T. S. Ratiu. *Introduction to Mechanics and Symmetry*. Springer, 1999.

[37] T. McGeer. Passive Dynamic Walking. *Int. J. of Robotics Research*, 9(2):62–82, 1990.

[38] S. Nair and N. E. Leonard. Stable synchronization of mechanical system networks. *Journal of Control Optimization*, 47(2):661–683, 2008.

[39] S. J. Olney and C. Richards. Hemiparetic gait following stroke. part i: Characteristics. *Gait & Posture*, 4(2):136–148, 1996.

[40] O. Olusola, A. Vincent, and B. I. Njah. Global stability and synchronization criteria of linearly coupled gyroscope. *Nonlinear Dynamics and Systems Theory*, 13:258–269, 2013.

[41] V. Pomeroy, B. Evans, M. Falconer, D. Jones, E. Hill, and G. Giakas. An exploration of the effects of weighted garments on balance and gait of stroke patients with residual disability. *Clinical Rehabilitation*, 15:390–397, 2001.

[42] D. Reisman, H. McLean, J. Keller, K. Danks, and A. Bastian. Repeated split-belt treadmill training improves poststroke step length asymmetry. *Neurorehabilitation*, 27, Feb 2013.

[43] D. S. Reisman, R. Wityk, K. Silver, and A. J. Bastian. Split-belt treadmill adaptation transfers to overground walking in persons poststroke. *Neurorehabil Neural Repair*, 23(7):735–744, Sep 2009.

[44] J. Ruffieux, M. Keller, B. Lauber, and W. Taube. Changes in standing and walking performance under dual-task conditions across the lifespan. *Sports Medicine*, 2015.

[45] M. K. Seeley, B. R. Umberger, J. L. Clasey, and R. Shapiro. The relation between mild leg-length inequality and able-bodied gait asymmetry. *Journal of Sports Science and Medicine*, 9:572–579, 2010.

[46] H. Skinner and R. Barrack. Ankle weighting effect on gait in able-bodied adults. *Archives of Physical Medicine and Rehabilitation*, 71:112–115, 1990.

[47] G. Sterman, A. Goldhaber, and R. Shrock. *Symmetry and Modern Physics : 1999 Yang Retirement Symposium*. World Scientific, 2003.

[48] M. T. Torbey and M. H. Selim. *The Stroke Book*. Cambridge University Press, 2007.

[49] G. Torres-Oviedo, E. Vasudevan, L. Malone, and A. J. Bastian. Locomotor adaptation. *Progress in Brain Research*, 2011.

[50] Y.-R. Yang, R.-Y. Wang, Y.-C. Chen, and M.-J. Kao. Dual-task exercise improves walking ability in chronic stroke: A randomized controlled trial. *Archives of Physical Medicine and Rehabilitation*, 88, October 2007.

[51] K. Y. M. Yeung, J. Chee, Y. Song, J. Kong, and D. Ham. Symmetry engineering of graphene plasmonic crystals. *Nano Letters*, 2015.

[52] D. W. Zaidel and M. Hessamian. Asymmetry and symmetry in the beauty of human faces. *Symmetry*, 2:136–149, 2010.

[53] Zenyu. A detail of the Raimondi Stela [online image]. retrieved September 25, 2015 from Wikimedia, July 2005.

Appendices

Appendix A: Copyright Permission for Chapter 3

Nonlinear Dynamics and Systems Theory
An International Quarterly Journal of Research and Surveys
Editor-in-Chief A.A.Martynyuk
The S.P.Timoshenko Institute of Mechanics, Nesterov Str. 3,
03680 MSP, Kiev-57, UKRAINE

Tel: ++38044-446-6140 **Fax: ++38044-446-0319** **E-mail: anmart@stability.kiev.ua**

Nonlinear Dynamics and Systems Theory
ISSN 1562-8353 (print) and ISSN 1813-7385 (online)
Impact Factor from SCOPUS for 2013: SNIP – 1.108, IPP – 0.809, SJR – 0.496

To whom it may concern,

Permission is granted to HARIS MURATAGIC for the use of content from:

> *Handzic, H. Muratagic, and K. B. Reed. Passive kinematic synchronization of dissimilar and uncoupled rotating systems. Nonlinear Dynamics and Systems Theory, 2015.*

As an author of the work, you are granted the use of this material to be reused, in part, for the completion of the Master's Thesis entitled "Passive Symmetry in Rotating Systems and Walking".

Sincerely,

A.A.Martynyuk

_____

Anatoly A. Martynyuk
Editor-in-Chief,
Nonlinear Dynamics and Systems Theory

Appendix B: KMC Derivation for Collision Events

This sections shows the complete derivation of the Kinematically Matched Coefficients of the heel strike equations in a PDW. We begin with the Nine Mass Model and show it's two link phase walking, shown in Figure B.1.

B.1 Nine Mass Model

First, in order to model the system in Figure B.1 into a compass gait, we set the shank masses ($ms1L, ms2L, etc.$) and angle $q3$ to zero. This allows the system to become a two-link model, similar to that of an inverted double pendulum system. I reference [25] and follow a similar procedure to begin calculating the pre-heel strike and post-heel strike velocity, then I will gather the KMCs necessary for synchronization. We begin by applying the conservation of angular momentum after gathering the pre-collision velocities from the free swinging system.

This particular PDW model contains two joint angles, resulting in two 2x2 matrices, one for the pre-collision and one for the post-collision.

$$Q_{pre}\dot{\theta}_{pre} = Q_{post}\dot{\theta}_{post} \tag{B.1}$$

where,

$$[Q_{post}]^{\check{2},\check{2}}_{\text{sym}} = \begin{bmatrix} Q_{11}^{post} & Q_{12}^{post} \\ Q_{21}^{post} & Q_{22}^{post} \end{bmatrix} \tag{B.2}$$

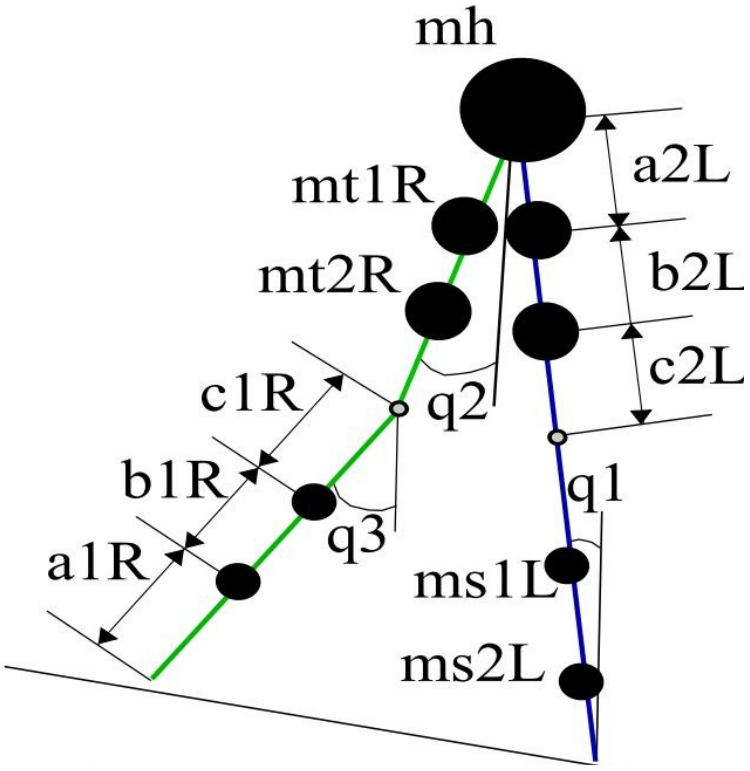

Figure B.1: A nine mass PDW model used to develop KMCs of the compass gait.

$$[Q_{pre}]^{\check{2},\check{2}}_{\text{sym}} = \begin{bmatrix} Q^{pre}_{11} & Q^{pre}_{12} \\ Q^{pre}_{21} & Q^{pre}_{22} \end{bmatrix} \tag{B.3}$$

The KMCs that are present within the collision matrices are shown in equations B.4-B.9.

$$\begin{aligned} Q^{pre}_{11} = {} & LL*mt2R*cos(q1-q2)*(a1R+b1R+c1R+c2R) \ + \ ... \\ & mt1L*cos(q1)*(LR*cos(q2)-a2L*cos(q1))*(a1L+... \\ & b1L+b2L+c1L+c2L)+LL*mt1R*cos(q1-q2)*(a1R+... \\ & b1R+b2R+c1R+c2R)+LL*LR*mh*cos(q1-q2)+... \\ & mt1L*sin(q1)*(LR*sin(q2)-... \\ & a2L*sin(q1))*(a1L+b1L+b2L+c1L+c2L)-... \\ & mt2L*cos(q1)*(cos(q1)*(a2L+b2L)-... \\ & LR*cos(q2))*(a1L+b1L+c1L+c2L)-... \\ & mt2L*sin(q1)*(sin(q1)*(a2L+b2L)-... \\ & LR*sin(q2))*(a1L+b1L+c1L+c2L) \end{aligned} \tag{B.4}$$

$$\begin{aligned} Q^{pre}_{12} = {} & -a2R*mt1R*(a1R+b1R+b2R+c1R+c2R)-... \\ & mt2R*(a2R+b2R)*(a1R+b1R+c1R+c2R) \end{aligned} \tag{B.5}$$

$$\begin{aligned} Q^{pre}_{21} = {} & -a2L*mt1L*(a1L+b1L+b2L+c1L+c2L)-... \\ & mt2L*(a2L+b2L)*(a1L+b1L+c1L+c2L) \end{aligned} \tag{B.6}$$

$$\begin{aligned} Q^{post}_{11} = {} & a2L^2*mt1L+a2L^2*mt2L+b2L^2*mt2L \ + \ ... \\ & 2*a2L*b2L*mt2L-... \\ & LR*a2L*mt1L*cos(q1-q2)-LR*a2L*mt2L*cos(q1-q2)-... \\ & LR*b2L*mt2L*cos(q1-q2) \end{aligned} \tag{B.7}$$

$$
\begin{aligned}
Q_{12}^{post} = {} & mt2R*(a1R+b1R+c1R+c2R)^2+... \\
& mt1R*(a1R+b1R+b2R+c1R+c2R)^2 \ + \ ... \\
& LR^2*mh-LR*mt2L*cos(q2)*(cos(q1)*(a2L+b2L)-... \\
& LR*cos(q2))-LR*mt2L*sin(q2)*(sin(q1)*(a2L+b2L)-... \\
& LR*mt1L*cos(q2)*(LR*cos(q2)-a2L*cos(q1))+... \\
& LR*mt1L*sin(q2)*(LR*sin(q2)-a2L*sin(q1))
\end{aligned}
\tag{B.8}
$$

$$
Q_{21}^{post} = mt2L*(a2L+b2L)^2+a2L^2*mt1L \tag{B.9}
$$

$$
Q_{22}^{post} = -LR*cos(q1-q2)*(a2L*mt1L+a2L*mt2L+b2L*mt2L) \tag{B.10}
$$

After simplifying the above equations and applying several trigonometric identities, the pre-heel strike and post-heel strike matrices now only consist of 6 KMCs.

$$
[Q_{pre}]_{\text{sym}}^{\check{2},\check{2}} = \begin{bmatrix} f\,cos(\theta_1-\theta_2)+g & h \\ g & 0 \end{bmatrix} \tag{B.11}
$$

$$
[Q_{post}]_{\text{sym}}^{\check{2},\check{2}} = \begin{bmatrix} j+k\,cos(\theta_1-\theta_2) & i+k\,cos(\theta_1-\theta_2) \\ j & k\,cos(\theta_1-\theta_2) \end{bmatrix} \tag{B.12}
$$

The KMCs that are present within the collision matrices are shown in equations B.13-B.18.

$$
\begin{aligned}
f = {} & LL * mt2R * (a1R + b1R + c1R + c2R) + \ldots \\
& mt1L * LR * (a1L + b1L + b2L + c1L + c2L) + \ldots \\
& LL * mt1R * (a1R + b1R + b2R + c1R + c2R) + \ldots \\
& LL * LR * mh + mt2L * LR * (a1L + b1L + c1L + c2L)
\end{aligned}
\tag{B.13}
$$

$$
\begin{aligned}
g = {} & -mt1L * a2L * (a1L + b1L + b2L + c1L + c2L) - \ldots \\
& mt2L * (a2L + b2L) * (a1L + b1L + c1L + c2L)
\end{aligned}
\tag{B.14}
$$

$$
\begin{aligned}
h = {} & -a2R * mt1R * (a1R + b1R + b2R + c1R + c2R) - \ldots \\
& mt2R * (a2R + b2R) * (a1R + b1R + c1R + c2R)
\end{aligned}
\tag{B.15}
$$

$$
j = a2L^2 * mt1L + a2L^2 * mt2L + b2L^2 * mt2L + 2 * a2L * b2L * mt2L \tag{B.16}
$$

$$
k = -LR * (a2L * mt1L + a2L * mt2L + b2L * mt2L) \tag{B.17}
$$

$$
\begin{aligned}
i = {} & mt2R * (a1R + b1R + c1R + c2R)^2 + \ldots \\
& mt1R * (a1R + b1R + b2R + c1R + c2R)^2 + \ldots \\
& LR^2 * mh + LR^2 * mt2L + LR^2 * mt1L
\end{aligned}
\tag{B.18}
$$

Appendix C: ANOVA Results for Walking Study

Step Length ANOVA

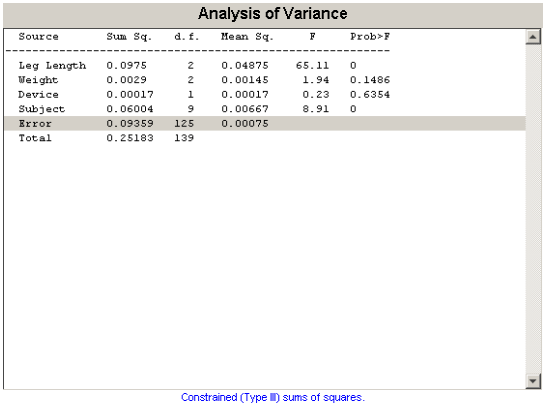

Analysis of Variance

Source	Sum Sq.	d.f.	Mean Sq.	F	Prob>F
Leg Length	0.0975	2	0.04875	65.11	0
Weight	0.0029	2	0.00145	1.94	0.1486
Device	0.00017	1	0.00017	0.23	0.6354
Subject	0.06004	9	0.00667	8.91	0
Error	0.09359	125	0.00075		
Total	0.25183	139			

Constrained (Type III) sums of squares.

Step Time ANOVA

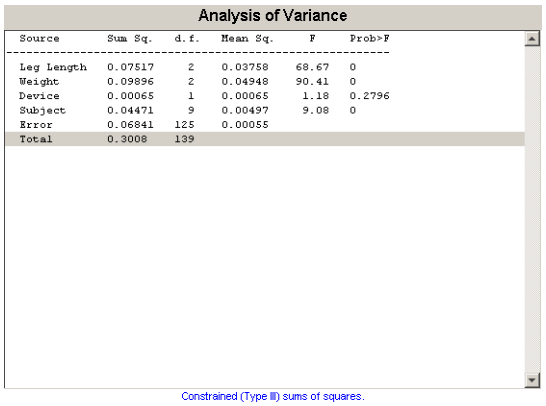

Analysis of Variance

Source	Sum Sq.	d.f.	Mean Sq.	F	Prob>F
Leg Length	0.07517	2	0.03758	68.67	0
Weight	0.09896	2	0.04948	90.41	0
Device	0.00065	1	0.00065	1.18	0.2796
Subject	0.04471	9	0.00497	9.08	0
Error	0.06841	125	0.00055		
Total	0.3008	139			

Constrained (Type III) sums of squares.

Figure C.1: The ANOVA analysis for the spatial temporal differences.

Vertical Force ANOVA

Analysis of Variance

Source	Sum Sq.	d.f.	Mean Sq.	F	Prob>F
Leg Length	337378.6	2	168689.3	111.52	0
Weight	57947.1	2	28973.6	19.15	0
Device	5026.4	1	5026.4	3.32	0.0707
Subject	112752.8	9	12528.1	8.28	0
Error	189073.5	125	1512.6		
Total	742639.1	139			

Constrained (Type III) sums of squares.

Push-off Force ANOVA

Analysis of Variance

Source	Sum Sq.	d.f.	Mean Sq.	F	Prob>F
Leg Length	25277	2	12638.5	19.85	0
Weight	4184.5	2	2092.2	3.29	0.0407
Device	284.6	1	284.6	0.45	0.505
Subject	132963	9	14773.7	23.2	0
Error	79602.6	125	636.8		
Total	244588.8	139			

Constrained (Type III) sums of squares.

Braking Force ANOVA

Analysis of Variance

Source	Sum Sq.	d.f.	Mean Sq.	F	Prob>F
Leg Length	61433.7	2	30716.8	34.33	1.30581e-012
Weight	297872.5	2	148936.2	166.47	5.70211e-036
Device	14779.4	1	14779.4	16.52	8.45256e-005
Subject	111490.5	9	12387.8	13.85	2.94456e-015
Error	111832.4	125	894.7		
Total	648093.8	139			

Constrained (Type III) sums of squares.

Figure C.2: The ANOVA analysis for the ground reaction force differences.